

Analysis of Retrofitted Concrete Columns using 3D Elastic-Plastic Modeling

Zaineb Al-Maadhidi

**A Thesis
in
The Department
of
Building, Civil and Environmental Engineering**

**Presented in Partial Fulfillment of the Requirements
for the Degree of
Master of Applied Science (Civil Engineering) at
Concordia University
Montréal, Québec, Canada**

October 2021

© Zaineb Al-Maadhidi, 2021

CONCORDIA UNIVERSITY

School of Graduate Studies

This is to certify that the thesis prepared

By: Zaineb Al-Maadhidi

Entitled: **Analysis of Retrofitted Concrete Columns using 3D Elastic-Plastic Modeling**

and submitted in partial fulfillment of the requirements for the degree of

Master of Applied Science (Civil Engineering)

complies with the regulations of this University and meets the accepted standards with respect to originality and quality.

Signed by the Final Examining Committee:

Prof. Khaled E. Galal Chair

Prof. Khaled E. Galal Examiner

Prof. Ashutosh Bagchi Examiner

Dr. Emre Erkmn Supervisor

Approved by

Ashutosh Bagchi, Chair of
Department of Building, Civil and Environmental Engineering

October 2021

Mourad Debbabi, Dean of
Faculty of Engineering and Computer Science

Abstract

Analysis of Retrofitted Concrete Columns using 3D Elastic-Plastic Modeling

Zaineb Al-Maadhidi

Fiber Reinforced Polymer (FRP) jacketing is frequently used to enhance the performance of concrete columns. The strength and ductility of a concrete column increase after FRP jacketing mainly because of concrete's improved behaviour under confinement. To achieve a reliable retrofit design, engineers often need to understand how much the performance is improved after FRP jacketing. For that purpose, numerical modelling is often necessary. Phenomenological elastic-plastic models are widely used for the numerical modelling of concrete because of their capability of representing 3D concrete behaviour considering permanent inelastic deformations. This research aims to implement an elastic-plastic model to simulate FRP-jacketed concrete columns. The 3D material model is validated against existing experimental data and comparisons with the results of models developed in ABAQUS software. It is shown that the proposed modelling approach is capable of providing an accurate behaviour of square concrete columns confined with reinforcements and FRP jackets under compression. After the validation of the model, a parametric study is conducted to illustrate the consequence of partial wrapping on the behaviour of retrofitted square concrete columns and to test the effect of FRP and concrete properties on the confined concrete strain. The obtained results from the parametric study are then used to acquire a suitable confined concrete strain equation/formula using a nonlinear regression technique. The core of this technique is based on an optimization method that finds the optimal coefficients for the proposed equation, helping in choosing the equation with the best fitting performance to the confined strain that is gained from the 3D material model. This proposed equation is recommended to improve the Canadian Standards by describing the impact of material properties on the confined concrete strain.

Acknowledgments

I would like to express my appreciation to my supervisor Dr. Emre Erkmen who was present to provide assistance with his knowledge, effort, time, and guidance. He was always there to support me during the research program.

I would like to acknowledge and express my sincere gratitude to my parents for their unconditional and endless support, inspiration, and encouragement with my studies and work. Even though we have been far away from each other, their prayers and wishes were with me every second of this journey. I doubt I would never do this without them. Special thanks to my brothers and cousins for their endless motivation and help.

I would like to thank the Canadian Standards Association (CSA) for their appreciated scholarship. Thank you for choosing me with the other students from all over Canada and allowing me to contribute to improving the Canadian Standards.

Last but not least, many thanks to my friends, colleagues and everyone who was there to encourage me with their kind words, much appreciated!

Thesis Published Work

Zaineb Khalid and Emre Erkmen. (2021, May 26-29). “Analysis of Retrofitted Concrete Columns using 3D Elastic-Plastic-Damage Modelling, ”*Canadian Society for Civil Engineering Annual Conference. 2021.* <https://csce2021.ca/wp-content/uploads/2021/05/CSCE-Updated-Program.210529.pdf>.

Contents

List of Figures	ix
List of Tables	xiii
1 Introduction	1
1.1 Overview	1
1.2 Problem Statement	2
1.3 Objective	2
1.4 Methodology	3
1.5 Outline of the Thesis	4
2 Literature Review	5
2.1 Introduction	5
2.2 Models for FRP Confined Concrete Columns	6
2.2.1 Compressive Strength Models	8
2.2.2 Stress-Strain Models	11
2.2.3 Finite Element Modeling	14
2.3 Case Studies	17
2.4 Literature Review Summary	19
3 Theories of Plasticity	20
3.1 Introduction	20
3.2 Elasto-Plastic Material Behavior	21

3.2.1	Stress-Strain Relationship	21
3.2.2	Frictional Block Models	23
3.2.3	The Tangent and Plastic Modulus	24
3.2.4	The Yield Criteria	25
3.2.5	Plastic Potential and Plastic Flow Rule	28
3.2.6	Consistency Condition	29
3.2.7	Principle of Plastic Work	29
3.2.8	Strain Hardening and Perfect Plasticity	30
3.3	Plasticity Model Component	32
3.3.1	Yield Surface	32
3.3.2	Hardening and Softening Functions	33
3.3.3	Potential Surface	35
4	3D Material Model (FORTRAN Code)	36
4.1	Introduction	36
4.2	Finite Element Type	37
4.3	Boundary Condition, Loading, and Meshing	38
4.4	Description of the Material Models and Parameters	39
4.4.1	Concrete Compression Model Implemented in FORTRAN	39
4.4.2	Reinforcement	44
4.4.3	FRP	44
5	Finite Element Model (ABAQUS)	45
5.1	Introduction	45
5.2	Finite Element Type and Meshing	45
5.3	Boundary Condition and Loading	46
5.4	Description of Material Model and Properties	47
5.4.1	Concrete	47
5.4.2	Reinforcement	51
5.4.3	FRP	52

6	Numerical Results	56
6.1	Introduction	56
6.2	Validation of the Numerical Model	56
6.2.1	Reinforced Concrete Column	56
6.2.2	Plain Concrete Columns Confined with FRP	57
6.2.3	Reinforced Concrete Columns Confined with FRP	58
6.3	Results of the 3D Material Model	60
6.4	Parametric Study	61
7	Implementation of Optimization Method to Obtain the Confined Strain Equation	64
7.1	Introduction	64
7.2	Gaps and Limitations in the Canadian Standards	65
7.3	Discussing the Gaps and Limitations in the Canadian Standards	66
7.4	The Proposed Nonlinear Regression Algorithm to Obtain the Maximum Confined Concrete Strain	68
7.4.1	Performance Measures	75
7.4.2	Results and Discussion	75
7.5	Summary Outcome	80
8	Conclusion and Future Work	82
8.1	Introduction	82
8.2	Summary Discussion	83
8.3	Recommendations for Future Work	84
	Bibliography	84

List of Figures

Figure 1.1	Damaged column due to an earthquake	2
Figure 2.1	External steel jacket	6
Figure 2.2	External FRP jack.	6
Figure 2.3	Confinement pressure distribution for noncircular section	7
Figure 2.4	stress-strain curves for confined concrete.	8
Figure 2.5	Modified distribution of confinement stress	10
Figure 2.6	Loading configuration considered in the validation.	11
Figure 2.7	Test setup of the specimens including a) ties at spacing 95mm b) ties at spacing 200mm c) specimen with FRP layers	18
Figure 3.1	Stress-strain curve for annealed material.	22
Figure 3.2	The behavior of a steel bar at different stress stages.	23
Figure 3.3	Types of stress-strain models	23
Figure 3.4	Frictional block model for a linear elastic-plastic material.	24
Figure 3.5	Plastic strain and tangent modulus.	24
Figure 3.6	The von Mises and Tresca yield surfaces in biaxial stress space.	27
Figure 3.7	The von Mises and Tresca cylinders in principal stress space.	27
Figure 3.8	The direction of the plastic strain.	28
Figure 3.9	The model of associative plasticity that obeys the principle of plastic work.	29
Figure 3.10	Perfectly plastic materials.	30
Figure 3.11	Isotropic hardening.	31
Figure 3.12	Kinematic hardening.	31

Figure 3.13	The split of hardening function into the hardening and softening part.	34
Figure 4.1	Column Components.	36
Figure 4.2	Finite element compatibility.	37
Figure 4.3	Boundary conditions and loading of the concrete column.	38
Figure 4.4	Laminates across thickness.	44
Figure 5.1	Finite element types used in ABAQUS.	46
Figure 5.2	Meshed column in ABAQUS.	46
Figure 5.3	Boundary condition and loading in ABAQUS.	47
Figure 5.4	Lam and Teng’s stress-strain model for FRP-confined concrete.	48
Figure 5.5	Reinforcement configuration in ABAQUS for BS2.	51
Figure 5.6	Lamina with unidirectional fibres.	52
Figure 5.7	Material properties required for FRP in ABAQUS.	53
Figure 6.1	Stress-strain curve for reinforced concrete column (BS2).	57
Figure 6.2	Stress-strain curve for plain concrete column wrapped with one FRP layer (BC1).	57
Figure 6.3	Stress-strain curve for plain concrete column wrapped with five FRP layers (BC5).	58
Figure 6.4	Stress-strain curve for RC column wrapped with one layer of FRP (BS1C1).	58
Figure 6.5	Stress-strain curve for RC column wrapped with three layers of FRP (BS1C3).	59
Figure 6.6	Stress-strain curve for RC column wrapped with five layers of FRP (BS1C5).	59
Figure 6.7	Stress-strain curve for RC column wrapped with three layers of FRP (BS2C3).	59
Figure 6.8	Stress-strain curve for RC column wrapped with five layers of FRP (BS2C5).	60
Figure 6.9	Stress-strain curves for retrofitted concrete columns using the 3D material model.	61
Figure 6.10	Stress-strain curve for BS2C5 with different mesh sizes using 3D material model.	62
Figure 6.11	Comparing the behavior of partially wrapped plain concrete column (BC1) with different spacing with fully wrapped and not wrapped cases using 3D material model.	62

Figure 6.12 Comparing the behavior of partially wrapped reinforced concrete column (BS2C5) with fully wrapped and not wrapped cases using 3D material model.	62
Figure 6.13 Different vertical spacing of FRP strips on the concrete column.	63
Figure 7.1 Maximum confined concrete strain vs number of layers of FRP from 3D material model and the Canadian Standards.	66
Figure 7.2 Stress-strain curves for plain concrete column wrapped with different number of FRP layers using the 3D material model.	67
Figure 7.3 Stress-strain curves for reinforced concrete column wrapped with different number of FRP layers using the 3D material model.	67
Figure 7.4 Changing some of the material parameters simultaneously in the structural analysis program.	72
Figure 7.5 Maximum strain obtained from 3D material model vs maximum strain obtained from Equation 1.	78
Figure 7.6 Maximum strain obtained from 3D material model vs maximum strain obtained from Equation 2.	78
Figure 7.7 Maximum strain obtained from 3D material model vs maximum strain obtained from Equation 3.	78
Figure 7.8 Maximum strain obtained from 3D material model vs maximum strain obtained from Equation 4.	78
Figure 7.9 Maximum strain obtained from 3D material model vs maximum strain obtained from Equation 5.	78
Figure 7.10 Maximum strain obtained from 3D material model vs maximum strain obtained from Equation 6.	78
Figure 7.11 Maximum strain obtained from 3D material model vs maximum strain obtained from Equation 7.	79
Figure 7.12 Maximum strain obtained from 3D material model vs maximum strain obtained from Equation 8.	79
Figure 7.13 Maximum strain obtained from 3D material model vs maximum strain obtained from Equation 9.	79

Figure 7.14 Maximum strain obtained from 3D material model vs maximum strain obtained from Equation 10.	79
Figure 7.15 Maximum strain obtained from 3D material model vs maximum strain obtained from Equation 11.	79
Figure 7.16 Maximum strain obtained from 3D material model vs maximum strain obtained from Equation 12.	79
Figure 7.17 Maximum strain obtained from 3D material model vs maximum strain obtained from Equation 13.	80
Figure 7.18 The Mean Square Error for all proposed equations.	80

List of Tables

Table 2.1	Mechanical properties of the materials.	17
Table 2.2	Experimental program.	18
Table 5.1	Mechanical properties of the carbon fiber.	55
Table 5.2	Mechanical properties of the resin epoxy matrix.	55
Table 5.3	The mechanical properties of the lamina composites as used in ABAQUS. . .	55
Table 7.1	The material parameters and the corresponding confined concrete strain and strength.	73
Table 7.2	The results obtained from nonlinear regression algorithm with respect to each possible equation.	77

Chapter 1

Introduction

1.1 Overview

The performance of the concrete columns is the primary factor affecting the structural response under extreme loading such as an earthquake. Upgrading the columns during their lifetime may be required due to damage or deterioration. Inadequate column behavior can happen due to inappropriate design or construction, and due to environmental factors such as heat expansion or earthquake events as shown in Figure 1.1. To prevent or avoid further failures, the columns may need retrofitting.

In recent times, using Fiber Reinforced Polymer (FRP) composites as wraps or jackets for concrete columns has become a very popular technique to improve concrete column's performance. It has been found that FRP jacketing increases the strength and ductility of the columns [Rousakis & Karabinis \(2012\)](#) [Parvin & Brighton \(2014\)](#). In addition, it is a simple installation so it can be used to retrofit the concrete columns which are damaged after construction.

In order to achieve a reliable design, engineers often need to understand the failure mechanisms of the structure. Describing the behavior of confined concrete under multiaxial compressive loading is one of the most challenging scopes in structural engineering. The elastic-plastic constitutive laws are not enough to model the load resistance and deformation capacity of confined concrete under multiaxial loads. Accordingly, more advanced sophisticated constitutive models are required.



Figure 1.1. Damaged column due to an earthquake [Ilki \(2006\)](#).

1.2 Problem Statement

Considering the collapse mechanisms and understanding the residual load capacity of the structure before and after possible retrofitting are required to be able to decide whether to continue with the operations, retrofit or demolish the structure.

Numerical modeling is often necessary to predict the behavior of the columns before and after applying the confinement techniques. Consequently, the design parameters can be improved and premature failure can be avoided. Besides, it is very important to use appropriate design standards for concrete columns reinforced with FRP composites for both fully and partially wrapped columns.

1.3 Objective

The global objective of the research work is to efficiently and accurately model concrete columns after retrofitting. To achieve this objective the following tasks are followed:

- (1) Adapt a 3D material model to capture the behavior of FRP confined reinforced concrete columns based on the coupled Elasto-Plastic model.
- (2) Predict the load capacity of FRP reinforced concrete columns.

- (3) Develop a finite element model using ABAQUS software for validation purposes.
- (4) Verify the accuracy of the numerical strategy by comparing the outcomes with experimental results from previous work and with ABAQUS results.
- (5) Recommend an optimization-based nonlinear regression to fill the gaps and limitations in the Canadian Standards (CSA S806-12) that are related to reinforced concrete columns confinement.

1.4 Methodology

In order to fulfil the objectives of this research, computational technology is developed to predict the behavior of both full and partial FRP wrapped concrete columns. A 3D material model is adopted based on the plasticity model to simulate the behavior of concrete beyond elasticity [Sarikaya & Erkmen \(2019\)](#). 3D modeling approaches are used to capture 3D stress distributions and their effect on material behavior. Also, the 3D material model has the ability to capture the confinement effect on the concrete structures.

The numerical model is developed by using the FORTRAN programming language. It is able to capture many possible modes of failure such as concrete crushing. It can easily be extended to capture reinforcement buckling and FRP tearing, however, the case studies were created such that these modes do not occur and therefore not considered in the analysis of this research.

The accuracy and efficiency of the numerical model are verified by comparing the outcomes of the model with experimental results from previous work. Moreover, a finite element model is developed in ABAQUS software for the confined concrete columns. The ABAQUS has the ability to analyze reinforced concrete columns that are wrapped with FRP. Accordingly, this software is a sufficient way to validate the results from the numerical strategy.

Filling in the gaps of limitations in the Canadian Standards by developing a nonlinear regression algorithm based on an optimization method to obtain the best suitable equation to describe the effect of FRP and concrete properties on the value of the maximum confined concrete strain. The nonlinear regression depends on the data acquired by the parametric study using the structural analysis program that is linked with the 3D material model in the FORTRAN program.

1.5 Outline of the Thesis

This thesis is organized into eight chapters including this chapter.

- **Chapter 2** reviews the confinement techniques and explains briefly some of the existing formulation and models for FRP confined columns. As well as a brief description of previous publications and works related to this field such as finite element modeling. The details of the case study are also provided at the end of this chapter.
- **Chapter 3** describes the theories of plasticity including the behavior of elasto-plastic materials and the component of plasticity models which are the yield surface, hardening and softening functions, and potential surface.
- **Chapter 4** describes the 3D material model including the concrete compression model which is implemented in FORTRAN codes.
- **Chapter 5** describes the finite element model in ABAQUS software in detail involving the concrete, reinforcement, and FRP.
- **Chapter 6** presents the main findings and results from the numerical methodology (FORTRAN code and ABAQUS). In this chapter, the 3D material model is validated against ABAQUS and experimental outcomes from previous studies. A parametric study is also conducted in terms of testing the behavior of partially wrapped square concrete columns under compression.
- **Chapter 7** summarizes the Canadian Standards gaps and limitations. In addition, it provides a nonlinear regression algorithm that helps in defining the change in the maximum confined strain after applying FRP layers by using the outcomes of the parametric study. The best equations which are recommended for the Canadian Standards to obtain the maximum confined strain are presented at the end of this chapter.
- **Chapter 8** summarizes the main findings and observations from this study. Also, it provides recommendations for future research work.

Chapter 2

Literature Review

2.1 Introduction

Confining concrete is a common practice in structural retrofitting applications, especially for bridge piers and columns. Those structures are strengthening due to unsuitable design or errors in the construction phase, and due to the modification of the structure use and the corresponding design loads. It has been shown very early that lateral confining stress can lead to a significant improvement in the strength of the concrete [Richart et al. \(1929\)](#). There are many ways to provide confinement to the concrete such as steel jackets, hoops, and FRP wrapping [Rousakis & Karabinis \(2012\)](#) [Zhang et al. \(2020\)](#) as shown in Figure 2.1 and Figure 2.2.

There is a difference between the lateral confinement provided by the FRP jacket and the steel. The lateral confinement pressure added by steel is constant following the yielding of steel. While the confinement pressure provided by the FRP jacket increases with the lateral strain of concrete as FRP does not yield. Furthermore, the FRP jackets apply a linear confining pressure which increases gradually until concrete ruptures as a result of its lateral dilation, whereas the reinforced steel exerts a constant confining pressure after yielding.

Recently, applying Fiber Reinforced Polymer (FRP) composites as wraps or jackets for concrete columns has become a well-known technique to enhance concrete column's behavior. It has been shown that FRP jacketing rises the strength and ductility of the concrete columns [Ozbakkaloglu & Saatcioglu \(2007\)](#) [Ilki et al. \(2008\)](#) [Rousakis & Karabinis \(2012\)](#) [Parvin & Brighton \(2014\)](#).



Figure 2.1. External steel jacket [Zhang et al. \(2020\)](#).



Figure 2.2. External FRP jack [Rousakis & Karabinis \(2012\)](#).

Moreover, it is a simple installation, lightweight, corrosion resistance, cost-effective, and a very good technique for retrofitting columns that have been already constructed [Bakis et al. \(2002\)](#) [Cheng & Karbhari \(2006\)](#) [Basalo et al. \(2012\)](#). Accordingly, FRP is superior in many aspects compared to other types of jacketing such as steel jacketing and concrete jacketing.

There are two types of FRP; glass FRP (GFRP) and carbon FRP (CFRP). Both types were used effectively in confining concrete columns as full jackets or partial confining strips [Ghernouti & Rabehi \(2011\)](#). Recently, It has been proved that FRP partial wrapping technique is an economical alternative to FRP full wrapping and this is working very well in enhancing concrete columns performance [Zeng et al. \(2018\)](#).

2.2 Models for FRP Confined Concrete Columns

The complexity of constitutive models for concrete varies from simple such as empirical and uniaxial models to complex such as plasticity and plasticity-damage models. In both aspects, an experimental calibration of the parameters is required but it is less in the case of the plasticity models. Accordingly, uniaxial models are more experimentally dependent since they are scenario-based models.

A large number of researchers have studied and simulated the behavior of the FRP confined

concrete columns. Most of the existing models are for circular sections since they are causing a uniform confining pressure which can be estimated based on the mechanical properties of the FRP and the diameter of the section. While the confining pressure around the perimeter of an FRP rectangular and square columns is not uniform. Accordingly, it is more difficult to use a mechanical solution to formulate the pressure distribution.

Several of the existing models for rectangular sections are quite similar to the circular section except for the shape factor introduced for non-uniform confinement and the definition of the equivalent diameter of the rectangular section. Figure 2.3 illustrates the confinement behavior at the corner of the rectangular section.

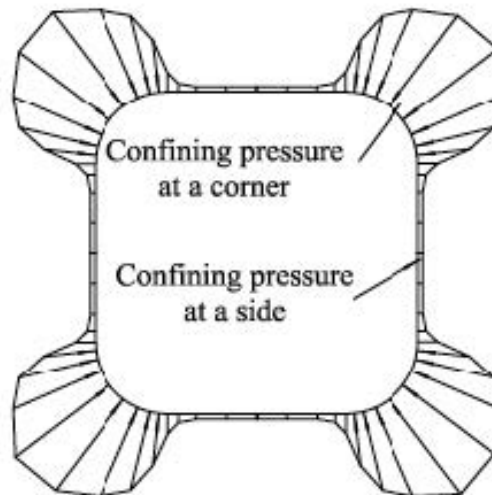


Figure 2.3. Confinement pressure distribution for noncircular section [Pham & Hadi \(2014\)](#).

Although many kinds of research have been carried out to study the behavior of plain concrete columns confined with FRP only, few models were proposed to account for the steel contribution and its interaction with FRP in the confined columns. In recent years, the implementation of FRP to rehabilitate and strengthen existing reinforced concrete (RC) columns has been widely used. In addition to the efficiency of FRP in increasing axial strength, shear capacity, and energy absorption capacity of reinforced columns, it protects the longitudinal steel bars from buckling. It has been found that the axial strength of columns confined with steel bars and FRP jackets is much higher than the axial strength of columns confined with FRP only [J.-Y. Lee et al. \(2004\)](#). Figure 2.4 shows the stress-strain relationships of confined concrete.

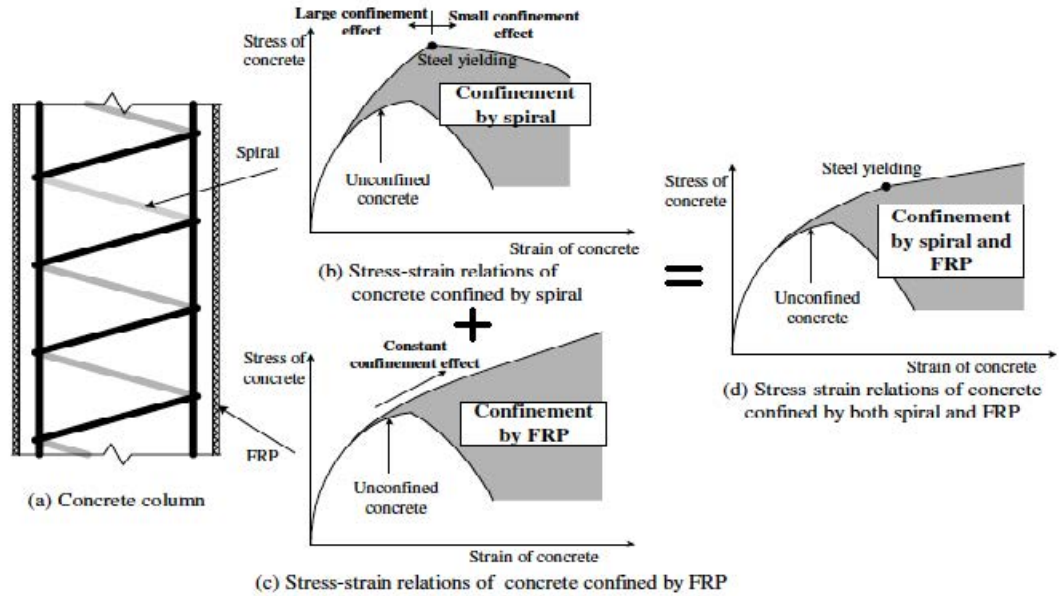


Figure 2.4. stress-strain curves for confined concrete [J.-Y. Lee et al. \(2004\)](#).

2.2.1 Compressive Strength Models

As it has been proven before, the strength of a concrete column can be strongly enhanced after applying FRP confinement. Accordingly, many types of research have been carried out to evaluate the confinement effect on the column's strength. [Jianguo et al. \(2008\)](#) developed a model to predict the concrete strength of rectangular columns that are confined with Fiber Reinforced Polymer (FRP). In addition, a design formula was suggested to calculate the ultimate load of the FRP-wrapped rectangular columns based on their investigated results. The confined core concrete strength f_{cc} was assumed to be a function of the uniaxial compressive strength of unconfined concrete and the effective confinement pressure f_r as given in the equation below:

$$f_{cc} = f_c + k f_r \quad (1)$$

where f_{cc} is the confined concrete strength and k is the confinement effectiveness coefficient, which is suggested to be a constant of 2.3 by fitting and regressing the test data from previous studies. [Jianguo et al. \(2008\)](#) also proposed a formula to calculate the ultimate load-carrying capacity

P_u of FRP strengthens columns as shown in the following expression:

$$P_u = P_{cu} + P_{su} \quad (2)$$

where P_{cu} is the compressive strength that is carried by the concrete and P_{su} is the compressive strength that is carried by the longitudinal reinforcing steel bars. A good correlation was obtained between the experimental results and the results from the proposed model and the design formula.

Pham & Hadi (2014) proposed a model to predict the strength of FRP confined rectangular concrete columns by focusing on the stress concentration at the corners of the section. Thus, the following equations were suggested to formulate a linear relationship between the normalized compressive strength of confined concrete f'_{cc} and the normalized confining pressure f_l :

$$\frac{f'_{cc}}{f'_{co}} = 0.68 + 3.91 \frac{f_{l,e}}{f'_{co}} \quad (3)$$

$$f_{l,e} = f_l k_c \quad (4)$$

$$k_c = \frac{\pi r}{b + h - r(4 - \pi)} \quad (5)$$

where k_c is the corner effect ratio, f'_{co} is the unconfined concrete strength, r is the corner radius, b and h are the column sides, and $f_{l,e}$ is the effective confining pressure. They concluded that the used model for stress prediction fits very well with the experimental results.

Although, the majority of the available models in the literature for rectangular and square confined columns with FRP focused on the confinement stress at corners only, Moodi et al. (2018) considered both the corners and neighbourhood areas as shown in Figure 2.5.

Hence, Moodi et al. (2018) modified the model proposed by Lam & Teng (2003a) using the whole algorithm and a widespread database to estimate the compressive strength of confined rectangular and square concrete columns with FRP. The effective strain coefficient of FRP k_ϵ and section shape coefficient k_a is considered as an individual coefficient $(k_\epsilon)_{new}$. Moreover, the modified model considered different increased strength values for samples with a compressive strength of less than 35 MPa or more than 35 MPa. The final proposed model after the optimization is summarized as

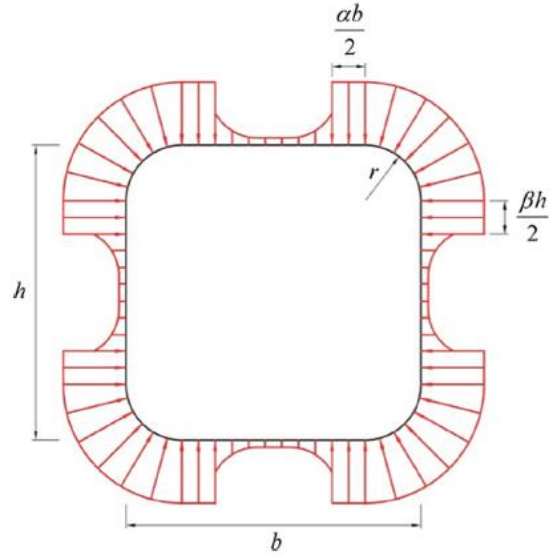


Figure 2.5. Modified distribution of confinement stress [Moodi et al. \(2018\)](#).

below:

$$f'_{cc} = f'_{co} \left(1 + 4.485(k_{\varepsilon})_{new} \frac{f_{l,a}}{f'_{co}} \right), f'_{co} \leq 35MPa \quad (6)$$

$$f'_{cc} = f'_{co} \left(1 + 2.478(k_{\varepsilon})_{new} \frac{f_{l,a}}{f'_{co}} \right), f'_{co} > 35MPa \quad (7)$$

$$(k_{\varepsilon})_{new} = \frac{\pi r + 0.0524b + 0.01h}{b + h - r(4 - \pi)} \quad (8)$$

where f'_{co} is the unconfined concrete strength, f'_{cc} is the confined concrete strength, $f_{l,a}$ is the confining pressure, b and h are the column sides, and r is the corner radius.

[Moodi et al. \(2018\)](#) also used Response Surface Methodology (RSM) to estimate the compressive strength of confined columns with FRP. It has been shown that RSM predicts compressive strength more accurately when compared with other models. The correlation coefficient has increased by about 34% and 26% for RSM and the modified model respectively.

[Zignago et al. \(2018\)](#) modified a material constitutive model to predict the load capacity of reinforced concrete confined columns. This model is capable to model the simultaneous confinement effect of reinforcement and FRP wrapping of reinforced concrete columns subjected to different loading conditions; axial concentric load, eccentric axial load, and a combination of axial and cyclic lateral loads as shown in [Figure 2.6](#)

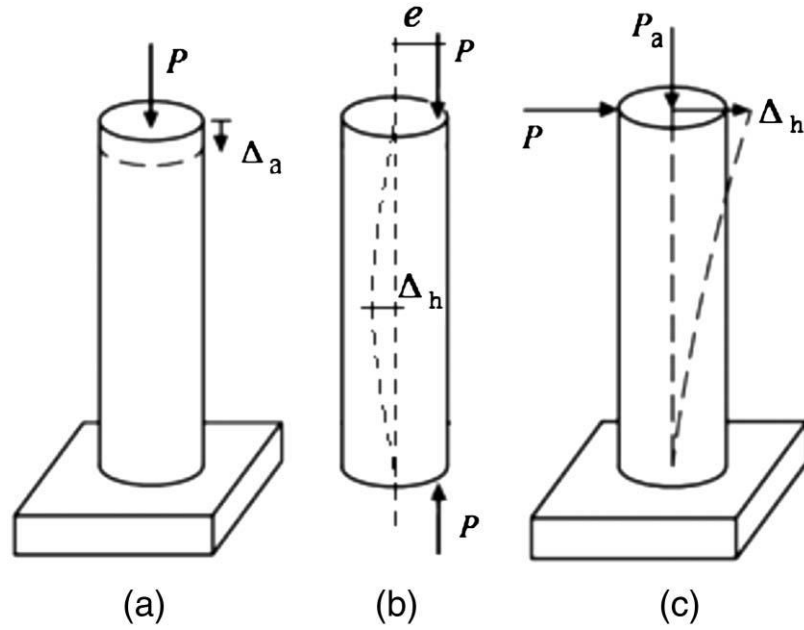


Figure 2.6. Loading configuration considered in the validation [Zignago et al. \(2018\)](#).

[Zignago et al. \(2018\)](#) also calculated the lateral confinement pressure f'_l as the summation of confinement pressure from transverse reinforcement steel $f_{l,steel}$ and FRP jackets $f_{l,FRP}$ as shown in the following equation:

$$f'_l = f_{l,steel} + f_{l,FRP} = \frac{1}{2}k_s\rho_s\sigma_s + \frac{1}{2}k_f\rho_f\sigma_f \quad (9)$$

where k_s is the coefficient of steel confinement effectiveness, ρ_s is the transverse steel reinforcement ratio, σ_s is the stress of the transverse reinforcement, and ρ_f is the stress of the FRP. The numerical simulation of the model was compared with the experimental results which were collected from the literature. It has been found that the new model provides an excellent estimation of the load-carrying capacity.

2.2.2 Stress-Strain Models

In general, the stress-strain models for concrete are classified into two groups; which are design-oriented models and analysis-oriented models. In the design-oriented models the compressive strength, ultimate axial strain, and stress-strain behavior of FRP confined concrete are estimated

using closed-form equations based on experimental results. Whereas, the stress-strain curves of FRP confined columns of the second group are created using the incremental numerical procedure. The analysis-oriented models have the advantage of considering the interaction between the confined concrete and the material that is used for the confinement. However, it is not used in the direct design because of the complexity of the incremental process.

Lam & Teng (2003a) proposed a new design-oriented stress-strain model based on existing test data and observations. They showed that the assumption that the rupture of FRP happens when the stress in the jacket reaches the tensile strength of the FRP material is invalid for confined columns with FRP. Accordingly, it was proved that the stress-strain model for confined columns with FRP must be based on the actual hoop rupture strain of FRP instead of the ultimate material tensile strain.

Lam & Teng (2003a) also studied different existing design-oriented stress-strain models then they improved the existing models by considering the effect of jacket stiffness. A new equation was proposed to calculate the compressive strength based on the largest databased that collected from the literature:

$$\frac{f'_{cc}}{f'_{co}} = 1 + 3.3 \frac{f_{l,a}}{f'_{co}} \quad (10)$$

where f'_{co} , f'_{cc} , and $f_{l,a}$ are the unconfined concrete strength, confined concrete strength, and confinement pressure provided by the FRP layer respectively. The ultimate strain equation was also proposed taking into account the FRP efficiency factor:

$$\frac{\varepsilon_{cu}}{\varepsilon_{co}} = 1.75 + 5.53 \frac{f_{l,a}}{f'_{co}} \left(\frac{\varepsilon_{frp}}{\varepsilon_{co}} \right)^{0.45} \quad (11)$$

where ε_{co} is the axial strain at the compressive strength of unconfined concrete, ε_{cu} is the axial strain of the confined concrete, and ε_{frp} is the hoop rupture strain. It has been concluded that the new oriented design stress-strain model is simple and suitable for direct use in design.

Fattah (2018) reviewed a variety of existing models of concrete columns confined with lateral steel and FRP that are available in the literature. Their performance was assessed based on experimental cases of square columns using stress-strain diagrams. Also, a statistical analysis was

conducted for theoretical peak strength and ultimate strain obtained from the existing models to improve their performance. [Fattah \(2018\)](#) also proposed a new model that overcomes the shortcomings found in the reviewed models to calculate the peak strength f'_{cc} , and the ultimate strain ε_{cu} :

$$f_{cc} = f'_c(1 + k_c k_{R1} \frac{f'_l}{f'_c}) \quad (12)$$

$$k_c = 2.66(\frac{f'_l}{f'_c})^{-0.6} w^{-0.2} \quad (13)$$

$$w = \frac{s}{d_s} + \frac{d_s E_s}{d_{Ls} E_{sl}} \quad (14)$$

where f'_c is the unconfined concrete strength, f'_l is the effective confining pressure, k_c is the strength enhancement parameter, w is a parameter for the longitudinal steel to lateral steel ratio, d_s is the longitudinal steel diameter, d_{Ls} is the lateral steel diameter, s is the tie spacing and k_{R1} is a parameter of the corner radius to width ratio. The ultimate strain is defined as:

$$\varepsilon_{cu} = \varepsilon_l + 0.75w^{-0.95}(\frac{f'_l}{f'_c})^{0.9} 1.1^{(5-\eta_f)} k_{R2} \quad \text{for } \eta_f \geq 5 \quad (15)$$

$$\varepsilon_{cu} = \varepsilon_l + 0.75w^{-0.95}(\frac{f'_l}{f'_c})^{0.9} 2^{(5-\eta_f)} k_{R2} \quad \text{for } \eta_f < 5 \quad (16)$$

where ε_l is the lateral concrete strain, k_{R2} is a parameter of the corner radius to width ratio, and η_f is the number of FRP layers. It was concluded that the proposed model has better correlations to the experimental curves than the existing models in the literature.

It is well known that in FRP- confined concrete the end restraints prevent the confined columns from the lateral expansion and generate a non-uniform strain of the FRP jacket over the column height. Accordingly, the peak axial stress and strain are underestimated. In order to eliminate the effect of end restraints, [Teng et al. \(2015\)](#) recalibrated the stress-strain model and proposed the following equation to calculate the lateral strain:

$$\frac{\varepsilon_c}{\varepsilon_{co}} = \{[1 + 0.75(\frac{-\varepsilon_l}{\varepsilon_{co}})]^{0.7} - \exp[-7(\frac{-\varepsilon_l}{\varepsilon_{co}})]\} \times (1 + 8\frac{\sigma_1}{f'_{co}}) \quad (17)$$

where ε_c and ε_l are the axial strain and the lateral strain of concrete respectively, ε_{co} is the axial strain of unconfined concrete at the compressive strength, f'_{co} is the unconfined concrete strength, and σ_1

is the lateral confining pressure.

Due to the change in the confinement effectiveness coefficient, the axial strain of concrete at the peak of axial stress of concrete under lateral confining pressure is calculated from the following equation:

$$\frac{\varepsilon_{cc}^*}{\varepsilon_{co}} = 1 + 20 \frac{\sigma_1}{f'_{co}} \quad (18)$$

where ε_{cc}^* is the axial strain at the peak axial stress of concrete under a lateral confining pressure. [Teng et al. \(2015\)](#) also modified the expression of the compressive strength of confined concrete f'_{cc}^* as shown below:

$$f'_{cc}^* = f'_{co} + 4\sigma_1 \quad (19)$$

The results obtained from the finite element analysis were compared with experimental stress-strain curves. It has been shown that there is a good agreement between the results, so the provided finite element approach has the ability to predict the behavior of reinforced concrete and plain concrete columns confined with FRP.

2.2.3 Finite Element Modeling

During the first decade of the 21st century, several attempts have been done to model concrete columns that are confined with FRP using the finite element method. This method has the ability to deal with nonlinear geometries and capture the interaction of different materials. On the other hand, using finite element modeling of confined columns is a challenging task since the definition of the concrete material model must be defined accurately to represent the volumetric behavior of concrete subjected to triaxial stress states.

For finite element structural modeling purposes, several uniaxial stress-strain relationships have been developed for confined concrete including the works of [Saatcioglu & Razvi \(1992\)](#) [Attard & Setunge \(1996\)](#) [Isleem et al. \(2018\)](#) . Such models require a prior estimate of the confinement

pressure which however depends on the local stress distribution. On the other hand, elastic-plastic-damage based constitutive laws have been applied extensively for the description of the progressive failure of concrete.

3D elasto-plastic damage models have the capability of capturing the confined concrete behavior naturally as a result of the stress distribution as the stress-strain relations are developed considering the multi-axial states. Furthermore, the evolution of the internal parameters in phenomenological plasticity and damage models can be related to underlying mechanisms within the material in a thermodynamically consistent manner, e.g., development of slip bands and dislocation systems causing plastic deformations or void nucleation and crack development causing stiffness degradation. Initial attempts to merge elastoplastic and damage constitutive models can be found in [Lemaitre \(1985\)](#) [Simo & Ju \(1987\)](#) . Other coupled plasticity and damage models include the works of [Klisiński & Mroz \(1988\)](#), [Benallal et al. \(1988\)](#), [Lubliner et al. \(1989\)](#), [Yazdani & Schreyer \(1990\)](#), [Meschke et al. \(1998\)](#), [Grassl & Jirásek \(2006\)](#), and [Voyiadjis et al. \(2008\)](#).

An efficient coupled elastoplastic damage model that is capable of simulating the behavior of plain concrete was also developed by [J. Lee & Fenves \(1998\)](#). Recently, [Sarikaya & Erkmen \(2019\)](#) showed that the [J. Lee & Fenves \(1998\)](#) model can be captured as a special case within the framework of [Armero & Oller \(2000\)](#) by imposing a kinematic condition between the strain components. In both [Sarikaya & Erkmen \(2019\)](#) and [J. Lee & Fenves \(1998\)](#) a single failure surface, potential function and hardening/softening criterion can be adopted in order to characterize the inelastic behavior of concrete, providing an efficient computational framework.

Some other attempts for elasto-plastic-damage modeling of concrete can be found in [Grassl et al. \(2002\)](#); [Grassl & Jirásek \(2006\)](#); [Papanikolaou & Kappos \(2007\)](#). ABAQUS has included Elasto-Plastic-Damage models developed by [Lubliner et al. \(1989\)](#) and [Lam & Teng \(2003a\)](#) as modeling options.

[Mirmiran et al. \(2000\)](#) developed a nonlinear finite element model to analyse confined concrete with FRP. This model was generated based on a non-associative Drucker-Prager plasticity model which considers the pressure sensitivity of the materials. The concrete core was modelled as a solid element while the FRP jacket was modelled as linear-elastic membrane shell elements. A parametric program inside ANSYS software was developed for generating the mesh of different geometries and

material properties. It has been concluded that Drucker-Prager plasticity has the ability to predict the axial stress-strain response of the FRP confined columns effectively.

[Chakrabarti et al. \(2008\)](#) proposed a nonlinear finite element model to analyse the behavior of plain and reinforced concrete columns wrapped with FRP sheets. They used the ANSYS finite element software to simulate the model for the analysis of square and circular concrete columns and to predict the behavior of strengthened columns. The model was also used for a parametric study to measure the effect of FRP thickness, stiffness, and orientation on the confinement and concrete strength. The model was validated with other finite element and experimental results from previous works.

[Teng et al. \(2015\)](#) presented a three-dimensional finite element analysis for modeling the behavior of both; FRP -confined plain concrete and reinforced concrete circular columns. They obtained a local stress-strain model for concrete under uniform confinement to generate the input parameters for [Yu et al. \(2010\)](#) plastic damage model.

[Yu et al. \(2010\)](#) developed a modified damage plasticity model to simulate the behavior of confined concrete under non-uniform confinement. The modification of the model was within the theoretical framework of the damage plasticity model that is available in ABAQUS software. [Yu et al. \(2010\)](#) modified the damage parameter, strain hardening/softening and flow rule which are all confinement dependent. They also defined an effective confining pressure which is a special characteristic of non-uniformly confined concrete. One of the limitations of this model is the simulation of concrete confinement of the non-circular columns since it depends on some assumption

[Hany et al. \(2016\)](#) presented a modified concrete damage plasticity model (CDPM) for both normal and high strength FRP confined concrete. This modified model has the ability to predict the monotonic axial stress-axial strain behavior of confined concrete columns with FRP and reinforcement, as well as the lateral dilation of FRP confined concrete. After comparing the results of the modified model (CDPM) with experimental results of FRP confined concrete samples that available in the literature, it has been shown that there is a good agreement between the finite element results of the proposed model and the tested data.

[Farahmandpour et al. \(2017\)](#) also developed a damage plasticity model for concrete to describe the confinement sensitivity and dilation characteristics of concrete under a triaxial stress state. Most

of the existing constitutive models have many limitations, for example, the strain and stress cannot be fully analysed. Therefore, finite element code is required to generate a triaxial constitutive model of concrete. It has been concluded that the proposed model is valid through steel and FRP confinement with a wide range of confinement stiffness based on experimental validation.

2.3 Case Studies

In order to perform numerical modeling to predict the behavior of concrete columns before and after retrofitting, experimental data were obtained from the literature [Rousakis & Karabinis \(2012\)](#). This experimental program consisted of forty-two prismatic concrete columns. Most of the columns were strengthened by internal steel reinforcement and external FRP wrapping

All the tested columns have the same geometry of square cross-section of 200 mm, 320 mm height, and 30 mm corner radius. The specimens that were selected in this research for validation purposes were subjected to monotonic compression load until failure. The mechanical properties of concrete, steel reinforcement and carbon FRP (CFRP) are shown in Table 2.1.

Table 2.1. Mechanical properties of the materials.

Concrete	Compressive strength	25.5 MPa
	Elastic modulus	19.3 GPa
Steel	Nominal yield stress	500 MPa
	Elastic modulus	200 GPa
CFRP	Tensile modulus	240 GPa
	Thickness of each layer	0.117 mm
	Strain at failure	0.155

The reinforced concrete columns contain transverse and longitudinal reinforcement. The longitudinal reinforcement has a 14 mm diameter. Whereas, the transverse reinforcement has a diameter of 8 mm. Two spacing distances were used for transverse ties; 200 mm and 95mm, which symbolized S1 and S2, respectively. For the FRP wrapping, unidirectional carbon FRP sheets were implemented to some specimens for providing an external strength. Each sheet has a 300mm width

and the sheets are cut into a suitable length based on the number of layers that are used with an overlap of 200 mm only for the last external layer.

The application of the FRP composite required the preparation of the concrete surface. Accordingly, a coat of two components of epoxy resin was applied carefully on the concrete surface to ensure the proper underlay for the wrapping procedure. Two-component epoxy resin was also used to glue the composite sheets together by hand.

The following Table 2.2 shows the details and notation of the specimens used for the numerical validations and Figure 2.7 shows the experimental test setup of the specimens including the steel configuration.

Table 2.2. Experimental program.

Specimen label	Steel bars & ties	CFRP sheet layers	Jacket nominal thickness mm
B6	-	-	-
BS1	4 Φ 14 & 8 Φ /200	-	-
BS2	4 Φ 14 & 8 Φ /95	-	-
BC1	-	1	0.117
BC5	-	5	0.585
BS1C1	4 Φ 14 & 8 Φ /200	1	0.117
BS1C3	4 Φ 14 & 8 Φ /200	3	0.351
BS1C5	4 Φ 14 & 8 Φ /200	5	0.351
BS2C1	4 Φ 14 & 8 Φ /95	1	0.117
BS2C3	4 Φ 14 & 8 Φ /95	3	0.351
BS2C5	4 Φ 14 & 8 Φ /95	5	0.585

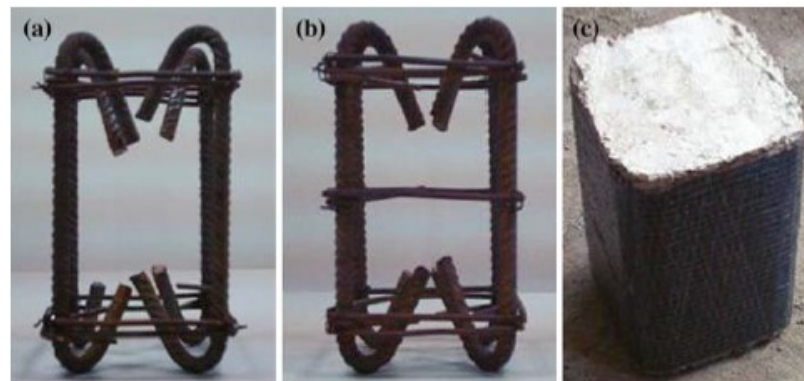


Figure 2.7. Test setup of the specimens including a) ties at spacing 95mm b) ties at spacing 200mm c) specimen with FRP layers Rousakis & Karabinis (2008).

2.4 Literature Review Summary

This chapter presented background information from the literature review about confining concrete techniques and the models which are used to model confined concrete with FRP. After reviewing some of the models that exist in the literature, two main points were noticed. The first point is most of the existing models are for confined concrete for circular column cross-sections. Secondly, few models were proposed to account for the steel contribution and its interaction with FRP in the confined columns. It is important to focus more on models for confined concrete that model square or rectangular cross-sections and capture the interaction of different materials such as FRP and steel reinforcement

Chapter 3

Theories of Plasticity

3.1 Introduction

The theory of linear elasticity is useful to model the materials that undergo small deformation that will return to their original state after removing the load. The energy consumed during the elastic deformation is stored as elastic strain energy which is recovered completely due to load removal.

Most of the materials suffer a permanent deformation when subjected to a load beyond its critical value which is called the yield stress. This deformation happens due to the dislocation and migration of the grain boundaries on the micro-level and it is irreversible. The distortion of an element is an energy dissipation process.

The elastic analysis does not give any information about the behavior of the materials after they reach the yield stress point. Therefore, the elastic model does not give the actual load that the structure can carry before collapsing.

From that perspective, the theory of plasticity was introduced to describe the irreversible deformation that remains upon complete unloading. Moreover, plastic analysis calculates the actual failure load of the structure. The failure load is critically greater than the elastic load capacity of the structure.

This chapter will illustrate the fundamental elements of plasticity theory. These elements include general stress-strain relations, yield condition, flow rule, consistency condition, the principle

of maximum plastic work, and isotropic and kinematic hardening.

3.2 Elasto-Plastic Material Behavior

3.2.1 Stress-Strain Relationship

The behavior of loaded materials is described in terms of the stress and strain relationship. There are two different ways to represent the applied stress. First calculating the stress-based on the original cross-sectional area A_o of the specimen which is called nominal stress σ_n Beer & Johnston (1992):

$$\sigma_n = \frac{F}{A_o} \quad (20)$$

while the other way is the true stress σ which is calculated based on the current cross-sectional area A .

$$\sigma = \frac{F}{A} \quad (21)$$

In which the area and the force are both changing with time. In the elastic range, there is very small elongation. Accordingly, the change in cross-sectional area is negligible so both definitions of stress are more or less equivalent. The strain is defined as the ratio of the change in length of the specimen to its original length Beer & Johnston (1992):

$$\varepsilon = \frac{L - L_o}{L_o} \quad (22)$$

where L is the current length and L_o is the original length which is continually changing.

The stress-strain diagram is obtained by plotting strain (ε) as abscissa and stress (σ) as an ordinate. The stress-strain curve for annealed material is divided mainly into two parts; elastic range and plastic range as illustrated in Figure 3.1. In the elastic region (from 0 to A'), the material recovers all strains after unloading. The curve is linear from 0 to A' with slope E , which is known as Young Modulus so the material obeys Hook's law.

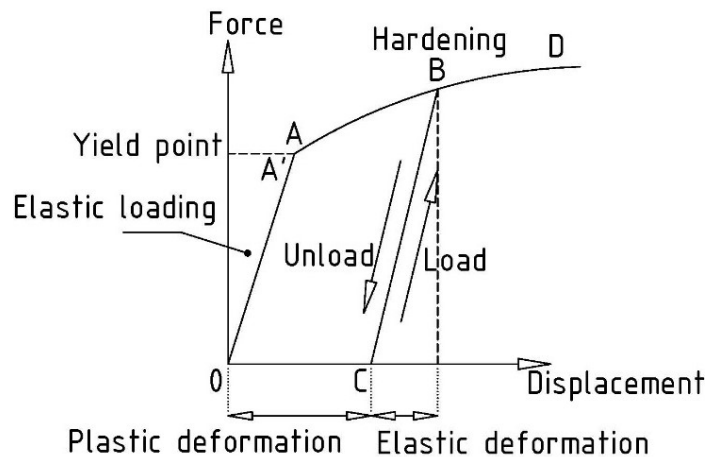


Figure 3.1. Stress-strain curve for annealed material.

Point A' is called the proportional limit while point A is the yield point where a small amount of permanent deformation is observed. As long as the material behaves elastically, the arrangement of the particles remained the same. Beyond the yield point, the material is classified as either brittle or ductile. For ductile materials, when yielding ends and load increases, the curve continues to rise from A to B but with a slope less than curve OA' , this behavior is called strain hardening. If the material is unloaded at point B it will return along path BC parallel to the original elastic line. This is known as elastic recovery.

The strain which remains upon unloading is irreversible and called plastic deformation which is due to the distortion of the particle arrange. Further increases in the load lead the curve to point D which is the ultimate stress value. After point D , the cross-sectional area starts to decrease. This behavior is called necking where the strength is dropped. Therefore, the material becomes weak and failure is occurred due to the development of shear stress. The change in the shape of a steel bar in different stress stages is shown in Figure 3.2.

There are many types of stress-strain models for elastic and plastic deformation as proposed in Figure 3.3. When a material deforms but still can take a load, it is called Elasto-plastic material and it follows the behavior of the first stress-strain curve (a) where both elastic and plastic curves are assumed linear. In (b) the work hardening is negligible so the yield stress is constant after yielding Chung & Lee (2018), such models are called perfectly plastic. The linear hardening behavior is represented in (c) and the rigid-perfectly plastic behavior is shown in (d).

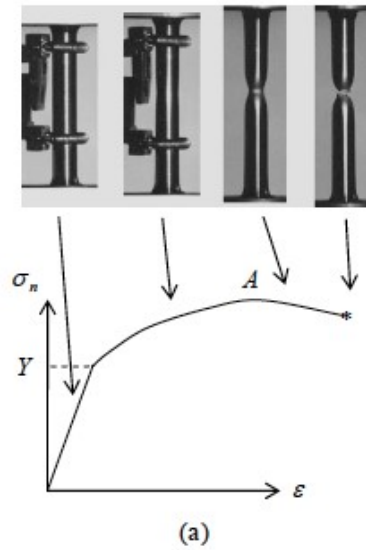


Figure 3.2. The behavior of a steel bar at different stress stages Kelly (2019).

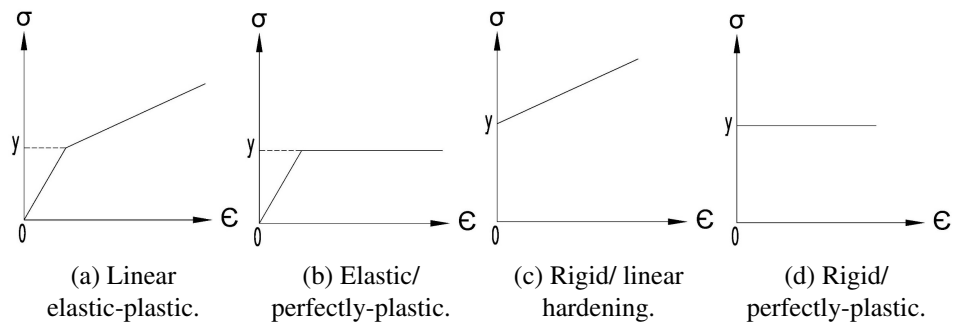


Figure 3.3. Types of stress-strain models

3.2.2 Frictional Block Models

The visual behavior of plastic materials can be shown by frictional block models Simo & Hughes (2006). The linear elastic-plastic model with linear strain hardening combines hardening spring with stiffness H , in parallel with the friction block. After yielding, an ever increases in stress is needed to be applied to keep the block moving and the elastic strain keeps occurring due to further elongation of the spring.

After that, the stress splits into two parts, one is called the yield stress which is carried by the moving block and the other one is known as the overstress which is carried by the hardening spring.

Figure 3.4 demonstrates the frictional block model for a linear elastic-plastic material with linear strain hardening; (a) stress-free, (b) elastic strain, (c) elastic and plastic strain, and (d) unloading behavior, where H is the plastic modulus.

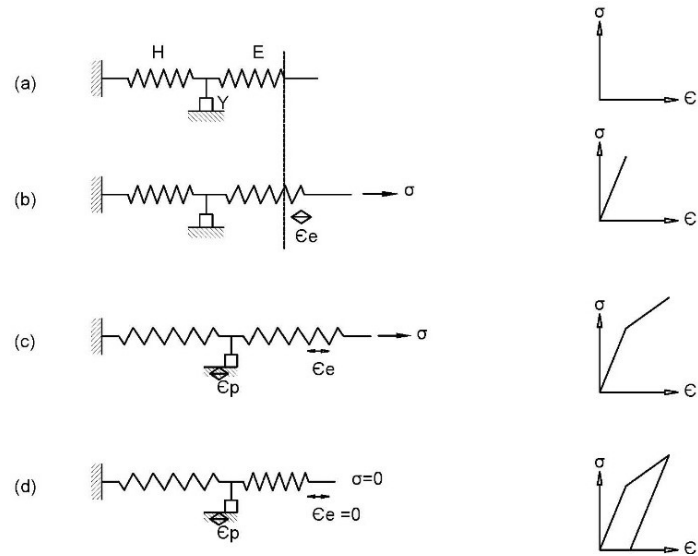


Figure 3.4. Frictional block model for a linear elastic-plastic material.

3.2.3 The Tangent and Plastic Modulus

In the elastic region, the stress and strain are relating to each other by Hook's law ($\sigma = E\varepsilon$) where E is the Young modulus. In the plastic region, the slope of the stress-strain curve is K which is known as tangent modulus that will change during plastic deformation as shown in Figure 3.5. At

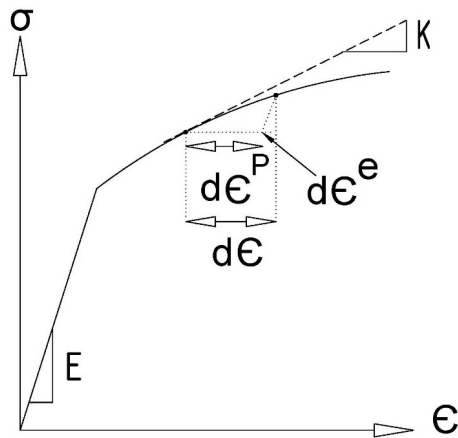


Figure 3.5. Plastic strain and tangent modulus.

any point of strain, the increment of stress $d\sigma$ is related to the increment of strain $d\varepsilon$ through [Simo & Hughes \(2006\)](#) [Borja \(2013\)](#):

$$d\sigma = Kd\varepsilon \quad (23)$$

After yielding, the total strain increment splits into elastic ε^e strain and plastic strain ε^P :

$$d\varepsilon = d\varepsilon^e + d\varepsilon^P \quad (24)$$

The stress and plastic strain increment are relating to each other through the plastic modulus H as shown below:

$$d\sigma = Hd\varepsilon^P \quad (25)$$

Finally, the tangent modulus is related to plastic modulus by the following equations:

$$\frac{1}{K} = \frac{1}{E} + \frac{1}{H} \quad (26)$$

$$\varepsilon = \varepsilon^e + \varepsilon^P = \frac{\sigma}{E} + \frac{\sigma - Y}{H} \rightarrow k = \frac{d\sigma}{d\varepsilon} = \frac{EH}{E + H} \quad (27)$$

Note: when:

- $H = 0$ Perfect plastic
- $H > 0$ Hardening
- $H < 0$ Softening

3.2.4 The Yield Criteria

A condition that defines the limit of elastic behavior and the beginning of plastic deformation under any possible combination of stress is called yield criterion or yield condition. This law is

not only applied to the first loading state, but also to reloading an element that unloaded from the previous loading state.

For the simple case of one-dimensional loading, the yield criterion is defined by the value of the stress that will cause permanent deformation. In other words, the yield criterion is graphically illustrated by a point. For two-dimensional loading, the yield will occur when the combination of the applied stress touches a curve between two loading directions [Borja \(2013\)](#).

In the case of three-dimensional loading, the plastic deformation will happen when the applied stress touches the yield surface. In general, the yield criterion is represented by the yield surface, if the applied load stays inside the surface the material behaves elastically. Once the stress touches the yield surface, plastic deformation will be produced. It has been found that the hydrostatic stress does not affect yielding, therefore the yielding depends only on the magnitude and direction of the deviatoric stress vector J_2 [Han & Reddy \(2012\)](#).

Many criteria were applied to determine whether a material has yielded, Tresca and von Mises were commonly used.

Tresca and von Mises Yield Criterion

This yield criterion is known as the theory of maximum shear strength. It is applicable for ductile materials such as metal. Tresca criterion assumed that the material yields when the maximum shear stress reaches a particular value. The yield surface was simulated as a hexagon as shown in [Figure 3.6](#). The plastic strain increment vector is directed along the normal to the side of the hexagon when the stress lies on one of the sides [Krabbenhøft \(2002\)](#). Therefore, plastic deformation is a pure shear in the direction of the maximum shear stress. Mohr's circle is used to solve for maximum shear stress and the material will fail if:

$$\sigma_1 - \sigma_3 \geq \sigma_0 \quad (28)$$

where σ_1 and σ_3 are the maximum and minimum normal stress, and σ_0 is the failure of stress in uniaxial loading.

Von Mises criterion (also known as the maximum distortion energy) is based on the Tresca

hypothesis but it takes into account that the hydrostatic stresses do not affect the material failure. Thus, only the deviatoric part of the stress tensor will change the shape and use it to construct the yield function for von Mises plasticity criterion [Han & Reddy \(2012\)](#).

The von Mises criterion is also referred to as J_2 plasticity since it can be written in the coordinate-independent format in terms of the second invariant J_2 of the deviatoric part of the stress tensor. The von Mises stress states that two stress states with equal distortion energy have an equal von Mises stress [Han & Reddy \(2012\)](#). The yield surface has a circular cylinder shape as shown in Figure 3.7.

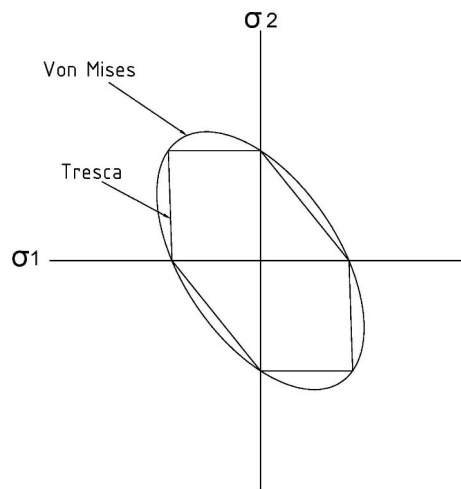


Figure 3.6. The von Mises and Tresca yield surfaces in biaxial stress space.

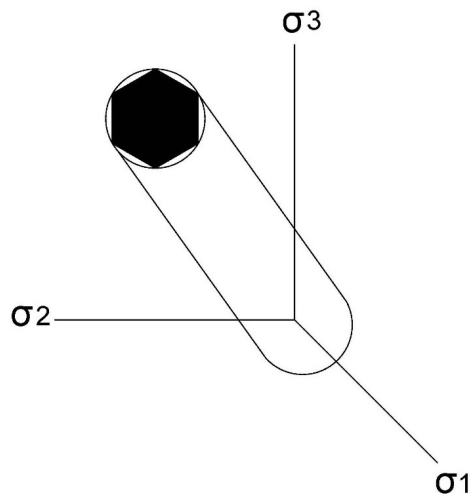


Figure 3.7. The von Mises and Tresca cylinders in principal stress space.

3.2.5 Plastic Potential and Plastic Flow Rule

The elastic strain increment is directly related to the stress increment by Hook's law. Therefore, it is important to relate plastic strain increment to the stress increment and current stress. The ratios of components of the plastic strain rate can be determined from the following equation [Ibrahimbe-govic \(2009\)](#) [Borja \(2013\)](#):

$$d\varepsilon_{ij}^p = d\lambda \frac{\partial g}{\partial \sigma_{ij}} \quad (29)$$

where $d\lambda$ is a positive scalar also it is called slip rate. This scalar is equal to zero in elastic unloading and g is known as plastic potential which may be the same as yield surface.

If the plastic potential is the same as the yield surface, the plastic flow rule is called an associated flow rule ($f = g$). Otherwise, it is called a non-associated flow [Han & Reddy \(2012\)](#).

The direction of plastic flow defines by the potential function which is usually the same as the yield function. The plastic flow rule states that during loading which causes the plastic deformation, all stresses should stay on the yield surface. As a result, the direction of the stress increments is tangential to the yield surface [Borja \(2013\)](#).

Besides, the direction of the elastic strain is also tangential to the yield surface because it produces stress increments. Whereas the plastic strain increments do not produce stress so their directions are normal to the yield surface as shown in Figure 3.8.

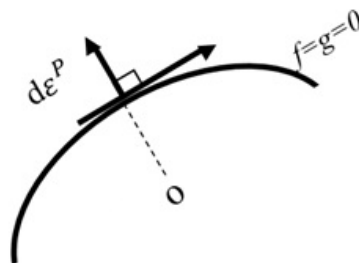


Figure 3.8. The direction of the plastic strain.

3.2.6 Consistency Condition

In order to obtain a whole relationship between stress and strain, the consistency condition should be assumed. For perfectly plastic materials (no hardening), consistency condition states that during loading the stress remains on the yield surface [Borja \(2013\)](#).

For strain hardening solids, the consistency condition means that the stress remains on the new yield surface (expanded, contracted, or translated). In other words, plastic loading is known as a consistency condition where loading from a plastically deforming state leads to another plastically deforming state [Han & Reddy \(2012\)](#) [Borja \(2013\)](#).

3.2.7 Principle of Plastic Work

Plastic work is also known as maximum plastic dissipation or the rate of plastic work. It states that the plastic work that is done in a given plastic strain rate has the maximum value. In particular, it is greater than the frictions work that is done by any state of stress not exceeding the yield limit.

The principle of maximum plastic dissipation is a vital component of the theory of plasticity. The values of the internal variables for plasticity can be obtained from the principle of plastic work. In the elastic range, the plastic dissipation is equal to zero. As a result, the values of the internal variables are zero [Han & Reddy \(2012\)](#). There are two considerable consequences of the principle of maximum plastic dissipation. First, the convexity of the yield surface (smooth surface). Secondly, the normality law which states that the plastic strain rate is normal to the yield surface [Figure 3.9](#).

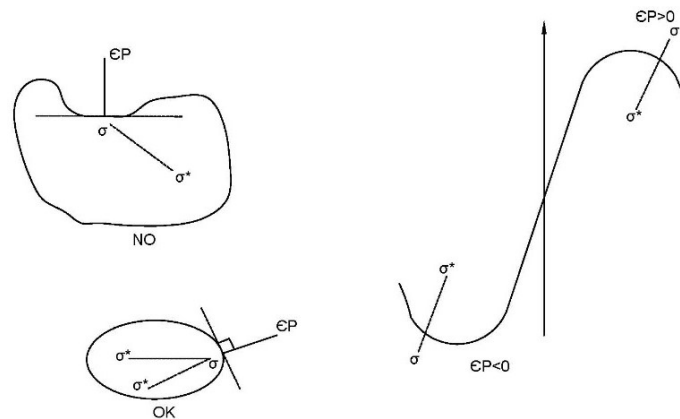


Figure 3.9. The model of associative plasticity that obeys the principle of plastic work.

3.2.8 Strain Hardening and Perfect Plasticity

In a one-dimensional (uniaxial test) case, the specimen will deform after yielding and then harden. Figure 3.10 illustrates the perfectly plastic materials where the material deforms at the yield point with no hardening.

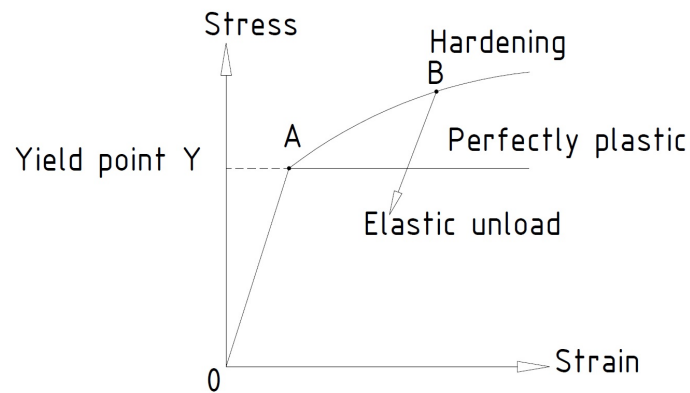


Figure 3.10. Perfectly plastic materials.

In the multiaxial case, strain hardening is when the yield surface changes in size, or location which depends on the complete history of plastic deformation since the previous loading. With the increase of stress beyond the yield point more plastic deformation will be produced and the material becomes stronger and more difficult to deform. There are two main hardening rules; isotropic hardening and kinematic (or anisotropic) hardening.

Isotropic Hardening

The rule of isotropic hardening assumed that the yield surface expands or contracts uniformly about centre of the original yield surface without a change in the shape as shown in Figure 3.11 Borja (2013).

The yield surface will be described by the following equation:

$$f = f(\sigma_{ij}) - R(\alpha) = 0 \quad (30)$$

where R represents the size of the yield surface depending on the plastic strain through the hardening internal variable α .

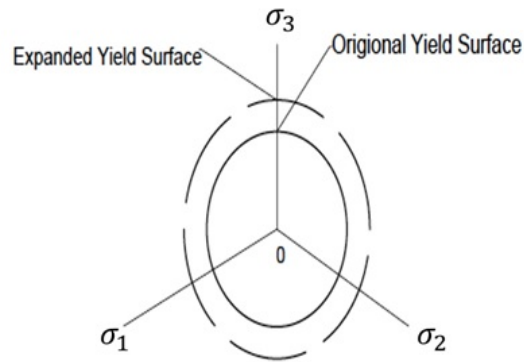


Figure 3.11. Isotropic hardening.

Kinematic Hardening

The rule of kinematic hardening assumed that the yield surface translates in the stress space during plastic flow as demonstrated in Figure 3.12. However, the shape and size of the yield surface will remain the same [Ibrahimbegovic \(2009\)](#) [Borja \(2013\)](#). It is important to note that the elastic range doesn't change and is simply translated. To capture the behavior of the kinematic hardening, back stress notation will be introduced. The yield surface will be described by the following

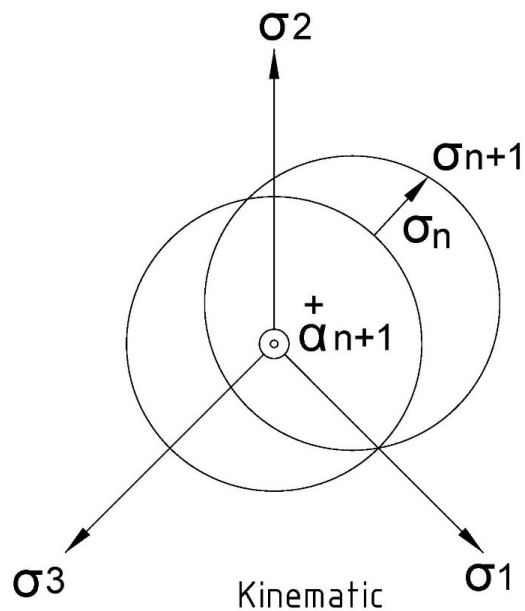


Figure 3.12. Kinematic hardening.

equation:

$$f = f(\sigma_{ij} - \alpha_{ij}) - R_0 = 0 \quad (31)$$

where α_{ij} represents the coordinates of the centre of the yield surface (back stress) and R_0 is a material constant that reflects the size of the original yield surface.

3.3 Plasticity Model Component

Many researchers suggested different theories and formulations for concrete modeling. It has been found that plasticity models are the most appropriate to capture the nonlinearities that grow as concrete loaded. The advantage of the plasticity theory is the ability to split the strain into elastic and plastic, the latter one is used to describe the inelastic behavior of concrete under compression.

The main plasticity model formulations are; yield surface (loading surface), the hardening and softening function, and plastic potential function.

3.3.1 Yield Surface

The yield/loading surface is used to describe the concrete triaxial stress state during plastic flow in terms of parameters that determine the size and shape of the surface. The yield surface proposed by [Menetrey & Willam \(1995\)](#) was the most popular in the literature. This yield surface formula is an extension of the Hoek and Brown failure criterion. It is described in terms of Haigh-Westergaard in stress space. Haigh-Westergaard coordinates are (ξ, ρ, θ) , where ξ is the hydrostatic stress invariant, ρ is the deviatoric stress invariant, θ is the deviatoric polar angle. The yield surface proposed by [Menetrey & Willam \(1995\)](#) is given by the following equation:

$$f = (\sqrt{1.5}\rho)^2 + q_n(k)m\left[\frac{\rho}{\sqrt{6}}r(\theta, e) + \frac{\xi}{\sqrt{3}}\right] - q_n(k)q_s(k) \leq 0 \quad (32)$$

The terms of the equation will be explained in detail in the coming chapter.

[Piscesa et al. \(2017\)](#) modified the [Menetrey & Willam \(1995\)](#) loading surface equation by introducing an additional variable α to control the frictional parameter and it is known as the frictional

driver parameter. It is used to accurately predict the peak and residual stresses for concrete under confinement. The new general form of loading surface is written as:

$$f = (\sqrt{1.5}\rho)^2 + q_n(k)\alpha m \left[\frac{\rho}{\sqrt{6}} r(\theta, e) + \frac{\xi}{\sqrt{3}} \right] - q_n(k)q_s(k) \leq 0 \quad (33)$$

The frictional parameter m will be modified by α based on the demanding peak stress and residual stress. The driver parameter is calculated by a linear interpolation function based on the softening function:

$$\alpha = (\alpha_{peak} q_s(k) + \alpha_{res}(1 - q_s(k))) \quad (34)$$

where α_{peak} is the frictional driver parameter at residual, while α_{res} is the frictional driver parameters at peak and both of the parameters are calculated using the following equations:

$$\alpha_{peak} = \frac{(f_{cc} - f_r)^2 - f_c'^2}{m f_r f_c'^2}; f_r = 0 \rightarrow \alpha_{peak} = \frac{2.5(f_c')^{0.79}}{m f_t} - \frac{2}{m} \quad (35)$$

$$\alpha_{res} = \frac{(f_{res} - f_r)^2}{m f_r f_c'^2}; f_r = 0 \rightarrow \alpha_{res} = 0 \quad (36)$$

Note that f_{cc} and f_{res} are the peak stress and residual stress for concrete under confinement respectively.

3.3.2 Hardening and Softening Functions

Hardening and softening functions can be described by means of the change of the location and size of the yield surface, that change is controlled by the hardening/softening parameter (k). Generally, the hardening parameter is selected to be the length of the plastic strain vector. Notwithstanding, this parameter has no ability to outline the increase of plastic deformation under multiaxial

compression stress. Therefore, many studies were done in the literature to modify the strain hardening material.

Grassl et al. (2002) presented a novel hardening law by using the volumetric plastic strain as a hardening parameter instead of the length of the plastic strain. Moreover, this hardening law is associated with non-linear plastic potential and a yield surface based on Hoek and Brown failure criteria. Accordingly, the novel hardening law is suitable for modeling the load resistance and deformation capacity of concrete in uniaxial, biaxial, and triaxial compression.

Grassl et al. (2002) proposed one hardening/ softening function $q(k)$ which is consisting of two functions (Figure 3.13); one representing the hardening $qh(k)$ and the other one representing the softening $qs(k)$ as shown below:

$$q(k) = qh(k)qs(k) \quad (37)$$

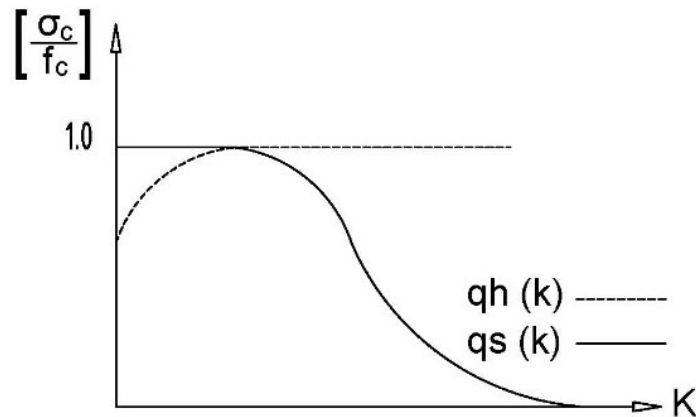


Figure 3.13. The split of hardening function into the hardening and softening part.

Since Grassl et al. (2002) doesn't propose a separate function for the hardening and softening, many studies were carried out to propose such a function.

Carrazedo et al. (2013) proposed new equations to define the hardening and softening functions in the ascending and descending branches based on the stress-strain model. Those functions are simpler than others and can model the behavior of a different type of concrete. The hardening parameter is selected following the suggestion of Grassl et al. (2002). It has been shown that the volumetric strain can be decoupled in elastic and plastic components and the plastic volumetric

strain is similar for all concrete types at the peak stress. Thus, the volumetric plastic strain is not used directly as a hardening parameter, a normalized parameter was used instead as shown below:

$$k = \frac{\varepsilon_v^p}{\varepsilon_{vo}^p} \quad (38)$$

In the above equation, ε_v^p is the volumetric plastic strain while ε_{vo}^p is the volumetric plastic strain at peak stress for uniaxial compression.

[Carrazedo et al. \(2013\)](#) proposed an equation for the descending branch:

$$q_h(k) = 1; \quad q_s(k) = \frac{C_3}{(k-1)^2 + C_3} \quad (39)$$

where C_3 is a parameter that affects the shape of the hardening function in the descending branch. Note that changeover between the hardening $q_h(k)$ and the softening $q_s(k)$ curve occurs when $q_h = q_s = 1$ to ensure continuity and obtain a smooth transition.

3.3.3 Potential Surface

Most of the quasi-brittle materials have a non-associated flow rule, concrete is one of them. In the situation of non-associated flow, the plastic potential function plays an important role in the plastic constitutive models. In general, the plastic potential function is used to govern the direction of the plastic strain vector. Hence, it controls the accumulation of the plastic volumetric strain.

[Grassl et al. \(2002\)](#) suggested a quadratic form for the plastic potential surface using the coordinates in the Haigh-Westergaard stress space.

[Papanikolaou & Kappos \(2007\)](#) proposed a new function for the plastic potential surface that characterise by Lode-angle (θ) dependency and an adjustable order (n). This plastic potential surface allows the calibration of the strain under equibiaxial compression. Besides, it has a good ability to observe the softening behavior of concrete.

[Piscesa et al. \(2017\)](#) also introduced a plastic potential function with plastic dilation rate control parameter α_{po} in uniaxial and triaxial settings, which allows the plastic potential function to have a linear or non-linear plastic dilation rate.

Chapter 4

3D Material Model (FORTRAN Code)

4.1 Introduction

Computational technology is proposed to predict the behavior of FRP fully and partially wrapped concrete columns. The numerical 3D material model is developed by using the FORTRAN programming language. The 3D model is adopted and developed by [Sarikaya & Erkmen \(2019\)](#) based on elastic-plastic model to simulate the behavior of concrete beyond elasticity. This model has the ability to capture the confinement effect on the concrete structures. Also, each component of the modelled column (reinforcement, FRP and concrete bulk) can be introduced independently into the analysis as shown in Figure 4.1.

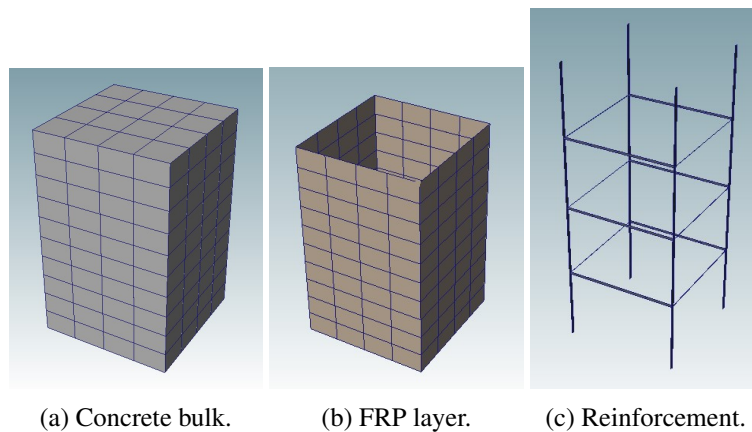


Figure 4.1. Column Components.

4.2 Finite Element Type

The concrete column model contains the concrete bulk, FRP jacketing as well as steel reinforcement which requires different types of elements to work together as they will be connected at the nodes. In the model developed, a four-node orthotropic shell-type element is used for the FRP sheets, a two-node beam-type element is used for the steel reinforcement and an 8-node solid element is used for the concrete bulk. The shell and solid elements contain drilling degrees of freedom so that all elements have compatible 6-DOFs as illustrated in Figure 4.2. All finite element types have been implemented and assembled in FORTRAN.

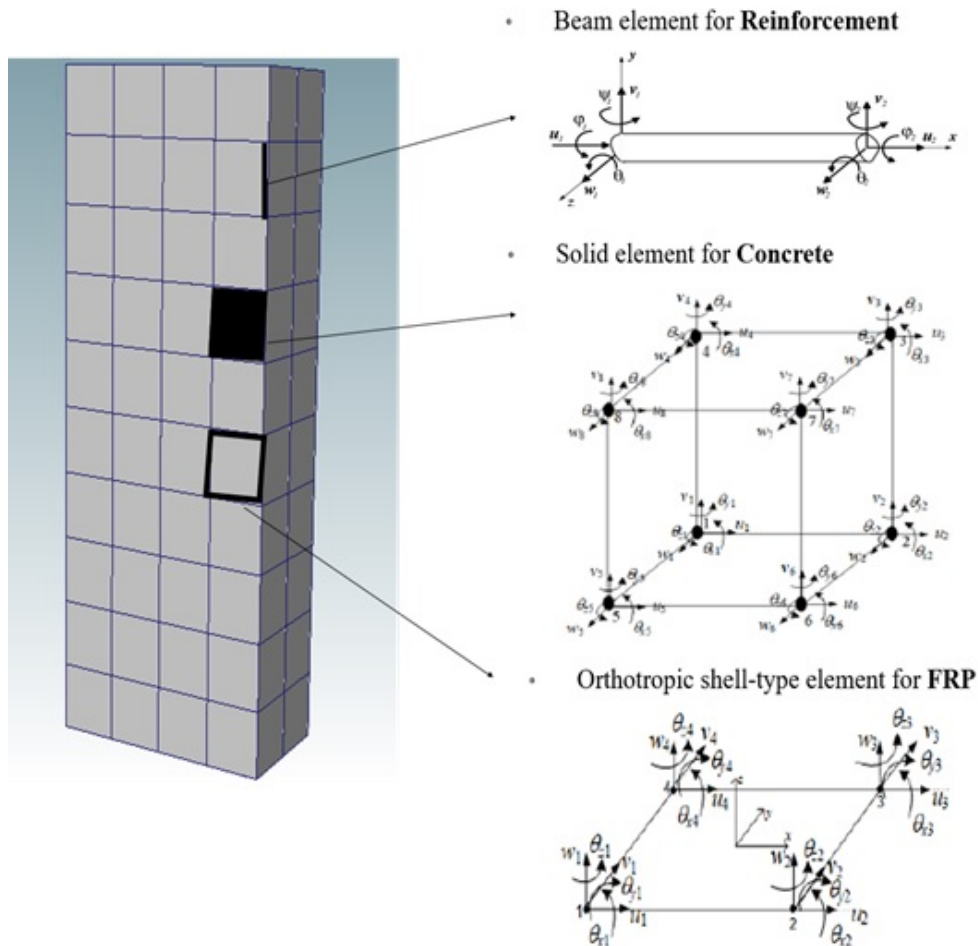


Figure 4.2. Finite element compatibility.

4.3 Boundary Condition, Loading, and Meshing

All the modelled columns in the program were fixed in the bottom in all directions while the nodes on the top were released except the middle point where the load was applied as shown in Figure 4.3. The load was applied based on the displacement control method on the middle top node on the direction Z . It was applied with a minus sign to follow the right direction. The displacement was increasing by 0.01 mm each step until failure. Each time the corresponding lamda λ was tabulated in order to obtain the load-deflection curve. The lamda is representing the load factor.

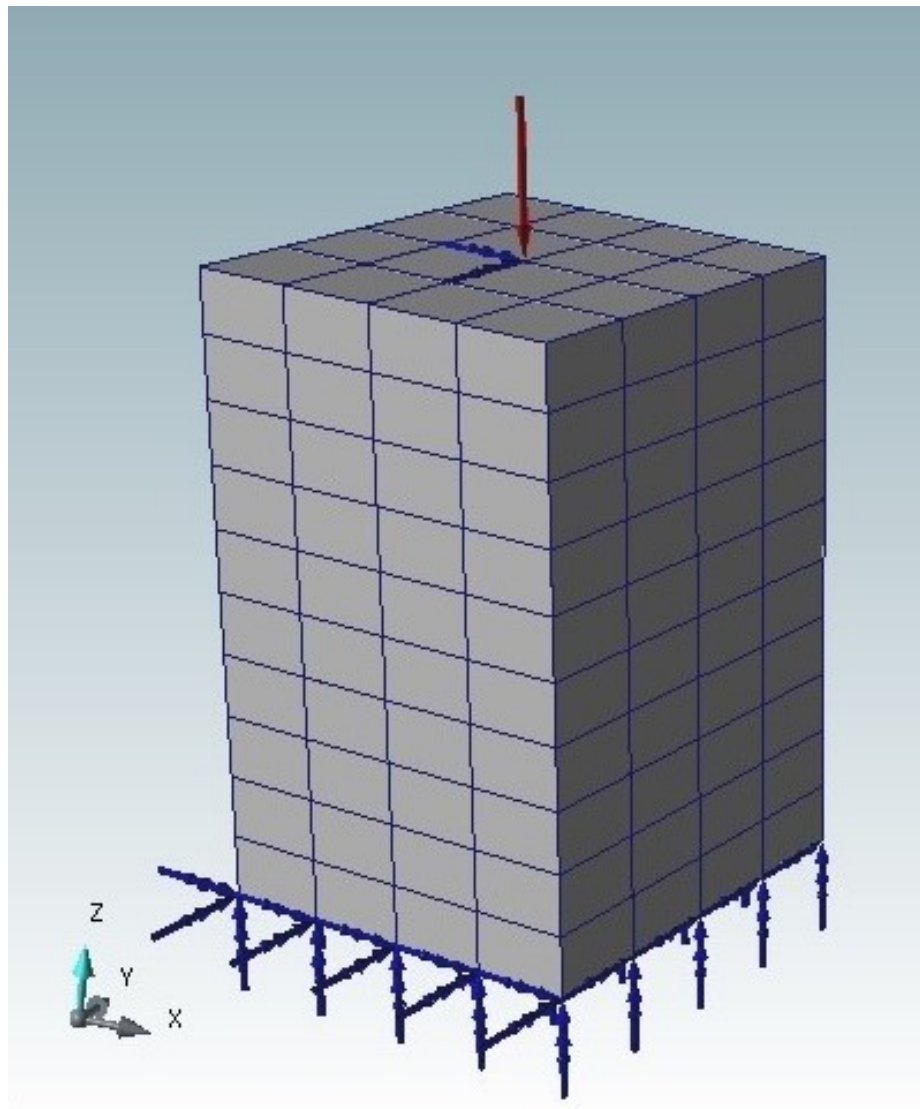


Figure 4.3. Boundary conditions and loading of the concrete column.

Meshing is the process where complex geometry is divided into simple elements by generating nodes and connecting them together. All the columns were modelled with 160 elements (32 mm mesh size). In order to test the model against mesh sensitivity, one column was modelled many times with different mesh sizes. The values are 40 mm, 53 mm, and 64 mm respectively. The behavior of the column with different mesh sizes was compared with the behavior of the 160 element-model.

4.4 Description of the Material Models and Parameters

4.4.1 Concrete Compression Model Implemented in FORTRAN

The plastic model that determines the envelope curve for stress-strain relationship consists of a potential surface, hardening law, which describes the deformation capacity in multiaxial compression, and a yield surface. The yield surface proposed by [Menetrey & Willam \(1995\)](#) was employed which is given as:

$$\phi^p(\xi, \rho, \theta, k_p) = (\sqrt{1.5}\rho)^2 + q_h(k_p)m\left[\frac{\rho}{\sqrt{6}}r(\theta) + \frac{\xi}{\sqrt{3}}\right] - q_h(k_p)q_s(k_p) \leq 0 \quad (40)$$

where q_h and q_s controls the shape and location of the loading surface and m can be written as:

$$m = 3 \frac{f_c^2 - f_t^2}{f_c f_t} \frac{e}{e + 1} \quad (41)$$

In which f_c is the uniaxial compressive strength, f_t is the uniaxial tensile strength taken herein as $0.09 f_c$. Both the plastic potential and the yield surface are constituted by using the unified co-ordinates in the Haigh–Westergaard stress space, which are based on the stress invariants. The three co-ordinates ξ , ρ and θ can be expressed as:

$$\xi = \frac{I_1}{\sqrt{3}f_c} \quad (42)$$

$$\rho = \frac{\sqrt{2J_2}}{f_c} \quad (43)$$

$$\cos 3\theta = \frac{3\sqrt{3}}{2} \frac{J_3}{J_2^{3/2}} \quad (44)$$

where:

$$I_1 = \sigma_{11} + \sigma_{22} + \sigma_{33} \quad (45)$$

$$J_2 = \frac{1}{6} [(\sigma_{11} - \sigma_{22})^2 + (\sigma_{22} - \sigma_{33})^2 + (\sigma_{33} - \sigma_{11})^2] + \tau_{12}^2 + \tau_{23}^2 + \tau_{31}^2 \quad (46)$$

$$\begin{aligned} J_3 = & -\left(\frac{I_1}{3}\right)^3 + \left(\frac{I_1}{3}\right)^2(\sigma_{11} + \sigma_{22} + \sigma_{33}) \\ & + \left(\frac{I_1}{3}\right)(\tau_{12}\tau_{12} + \tau_{13}\tau_{13} + \tau_{23}\tau_{23} + \sigma_{11}\sigma_{22} + \sigma_{11}\sigma_{33} + \sigma_{22}\sigma_{33}) - \tau_{13}\tau_{13}\sigma_{22} \\ & - \tau_{23}\tau_{23}\sigma_{11} - \tau_{12}\tau_{12}\sigma_{33} + 2\tau_{12}\tau_{13}\tau_{23} + \sigma_{11}\sigma_{22}\sigma_{33} \end{aligned} \quad (47)$$

The eccentricity e defined in the [Menetrey & Willam \(1995\)](#) model can be written as:

$$e = \frac{1 + \epsilon}{2 - \epsilon} \quad (48)$$

in which:

$$\epsilon = \frac{f_t f_b^2 - f_c^2}{f_b f_c^2 - f_t^2} \quad (49)$$

where f_b is the equibiaxial compressive strength taken herein as $1.5f_c^{-0.925}$. In Equation (40), $r(\theta)$ is the polar radius as:

$$r(\theta) = \frac{\nu(\theta)}{s(\theta) + t(\theta)} \quad (50)$$

In which:

$$\nu(\theta) = 4(1 - e^2)\cos^2\theta + (2e - 1)^2 \quad (51)$$

$$s(\theta) = 2(1 - e^2)\cos\theta \quad (52)$$

$$t(\theta) = (2e - 1)[4(1 - e^2)\cos^2\theta + 5e^2 + 4e]^{1/2} \quad (53)$$

Hardening and softening of concrete can be simulated by varying the shape and location of the loading surface during plastic flow. The variation is controlled by the hardening/softening parameter k_p . During the hardening range q_h in Equation (40) for concrete can be selected as [Papanikolaou & Kappos \(2007\)](#):

$$q_h(k_p) = k_o + (1 - k_o)\sqrt{1 - \left(\frac{\varepsilon_{vo}^p - k_p}{\varepsilon_{vo}^p}\right)^2} \quad (54)$$

where:

$$k_o = \frac{\sigma_{co}}{f_c} \quad (55)$$

In which σ_{co} is the uniaxial concrete stress at the onset of plastic flow. In Equation (54), ε_{vo}^p is the threshold value for the volumetric plastic strain at uniaxial concrete strength defined as:

$$\varepsilon_{vo}^p = \frac{f_c}{E_c}(1 - 2\nu) \quad (56)$$

where E_c and ν are the Young's modulus and Poisson's ratio for concrete, respectively. During softening range q_s in Equation (40) for concrete can be selected as [Papanikolaou & Kappos \(2007\)](#):

$$q_s(k_p) = \left(\frac{1}{1 + \left(\frac{n_1 - 1}{n_2 - 1}\right)^2}\right)^2 \quad (57)$$

where $n_1 = \frac{k_p}{\varepsilon_{vo}^p}$, $n_2 = \frac{\varepsilon_{vo}^p + t}{\varepsilon_{vo}^p}$ and $t = \frac{f_c}{15000}$. Note that f_c is considered in MPa. The potential function is again written in Haigh-Westergaard stress space and adopted herein from [Grassl et al.](#)

(2002) expressed as:

$$\Theta^p(\xi, \rho, q_p) = -A\left(\frac{\rho}{\sqrt{q_h(k_p)q_s(k_p)}}\right)^2 - B\frac{\rho}{\sqrt{q_h(k_p)q_s(k_p)}} + \frac{\xi}{\sqrt{q_h(k_p)q_s(k_p)}} \quad (58)$$

in which:

$$A = \frac{\psi_2 - \psi_1}{2(\rho_1 - \rho_2)} \quad (59)$$

$$B = \rho_1 \frac{\psi_1 - \psi_2}{(\rho_1 - \rho_2)} - \psi_1 \quad (60)$$

In Equations (59) and (60), ρ_1 and ρ_2 are the normalized deviatoric stress indicators at uniaxial and triaxial compressive strength, respectively as:

$$\rho_1 = \sqrt{\frac{2}{3}} \quad (61)$$

$$\rho_2 = \sqrt{\frac{2}{3}} \frac{|f_{cc} - \sigma_{pc}|}{f_c} \quad (62)$$

where f_{cc} is the triaxial compressive strength taken herein as $4.333 f_c$ and σ_{pc} is the lateral stress taken herein as f_c . On the other hand, ψ_1 and ψ_2 are the inclinations of the plastic strain vector under uniaxial and triaxial compressive strength, respectively given as:

$$\psi_1 = \sqrt{2} \frac{|\varepsilon_{3pu} - \varepsilon_{1pu}|}{\varepsilon_{vo}^p} \quad (63)$$

and

$$\psi_2 = \sqrt{2} \frac{|\varepsilon_{3pc} - \varepsilon_{1pc}|}{\varepsilon_{vo}^p} \quad (64)$$

In the above equation ε_{3pu} is the axial plastic strain component at uniaxial compressive strength,

which can be calculated as:

$$\varepsilon_{3pu} = \varepsilon_c - \frac{f_c}{E_c} \quad (65)$$

and ε_{1pu} is the lateral plastic strain component at uniaxial compressive strength, which is calculated as:

$$\varepsilon_{1pu} = \varepsilon_{2pu} = \frac{\varepsilon_{vo}^p - \varepsilon_{3pu}}{2} \quad (66)$$

In the equation above, ε_c is the total strain in the axial direction at uniaxial compressive strength. The axial plastic strain component at triaxial compressive strength ε_{3pu} is defined as:

$$\varepsilon_{3pu} = \varepsilon_{cc} - \frac{1}{E_c}(f_{cc} - 2v\sigma_{pc}) \quad (67)$$

and ε_{1pc} is the lateral plastic strain component at triaxial compressive strength, that is obtained from:

$$\varepsilon_{1pc} = \varepsilon_{2pc} = \frac{\varepsilon_{vo}^p - \varepsilon_{3pc}}{2} \quad (68)$$

For concrete it can be assumed that $\varepsilon_{cc} = \varepsilon_c(1 - 17\frac{\sigma_{pc}}{f_c})$, e.g., [Papanikolaou & Kappos \(2007\)](#) and generally σ_{pc} is taken as $\sigma_{pc} = f_c$, and thus in Equation (67), ε_{cc} becomes $\varepsilon_{cc} = 18\varepsilon_c$. The damage parameter φ is updated after every converged step. For this purpose, we have adopted the relationship given in [Grassl & Jirásek \(2006\)](#) defined as:

$$\varphi = (1 - e^{-C\frac{k_p}{\varepsilon_{vo}^p}}) \quad (69)$$

In which C is a parameter that is to be calibrated based on stiffness degradation.

It is important to note that we have adopted the potential function proposed by [J. Lee & Fenves \(1998\)](#), which is a special case of Equation (58) obtained by selecting $A = 0$ and $B = -\frac{1}{\alpha_p}$, i.e.

$$\Theta^p(\xi, \rho) = -B\rho + \xi - a \quad (70)$$

We have used $B = -6.25$, i.e., $\alpha_p = 0.16$ as suggested by [J. Lee & Fenves \(1998\)](#).

4.4.2 Reinforcement

The longitudinal and transverse reinforcement were considered as elastic perfectly plastic models. The steel nominal yield stress and the modulus of the elasticity were used in the program to model the reinforcement behavior.

4.4.3 FRP

The FRP layers were modelled as unidirectional lamina composites. The thickness of the layers was divided into two parts from the centre of the composite as shown in [Figure 4.4](#). The FRP material properties were entered in the program including the tensile modulus of elasticity, shear modulus, and the Poisson's ratio.

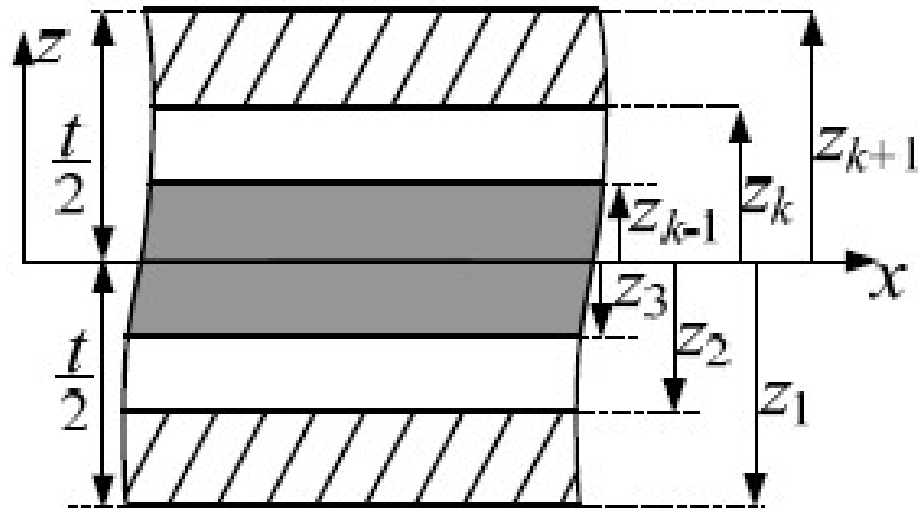


Figure 4.4. Laminates across thickness [Erkmen & Gottgens \(2018\)](#).

Chapter 5

Finite Element Model (ABAQUS)

5.1 Introduction

The finite element software ABAQUS is used to model the behavior of concrete columns confined with FRP wraps. The ABAQUS has the ability to analyze reinforced concrete columns wrapped with FRP. Accordingly, this software is a sufficient way to validate the results from the numerical strategy based on the coupled plastic damage model.

5.2 Finite Element Type and Meshing

In order to model the concrete column in ABAQUS, different element types have been used for each part of the column. Concrete, steel and FRP are the major materials used in the model. The bulk concrete is modelled as a homogeneous 8-node 3D brick element (C3D8R) and the longitudinal and transverse steel are modelled as linear truss element (T3D2) as shown in Figure 5.1. To model the FRP jacket, a shell element is used (S8R).

To model the interaction between the concrete and the reinforcement, an embedded region constraint is used. The embedded contact region is used to make sure that the number of translational degrees of freedom (DOF) at a node on the embedded element is identical to the number of translational degrees of freedom at a node on the host element (Compatible DOF). The reinforcement was embedded in the concrete which is considered the host region. Therefore, the concrete and

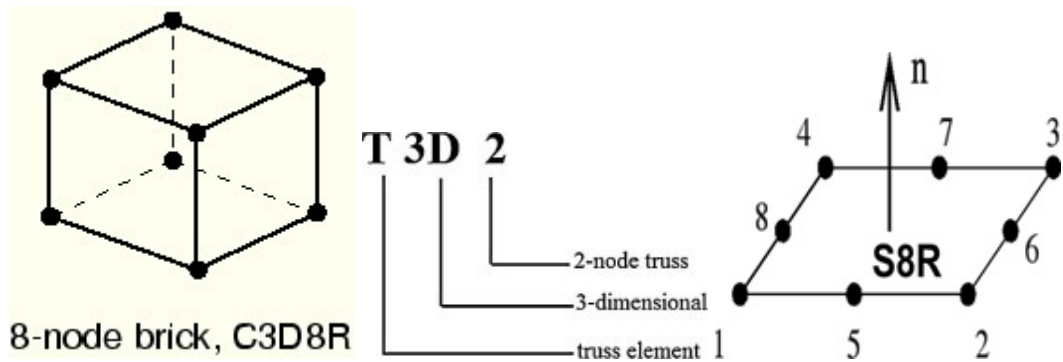


Figure 5.1. Finite element types used in ABAQUS [ABAQUS \(2008\)](#).

reinforcement share the same node where a perfect bond was assumed. The interaction between the concrete and the FRP jacket was considered as cohesive behavior contact.

All elements should have a compatible degree of freedom and share the same node. Accordingly, all the used elements in the model were assigned the same mesh size to ensure that the results obtained from the finite element model are accurate. The mesh size that used in the model is 32 mm to achieve good results with reasonable simulation speed as shown in Figure 5.2.

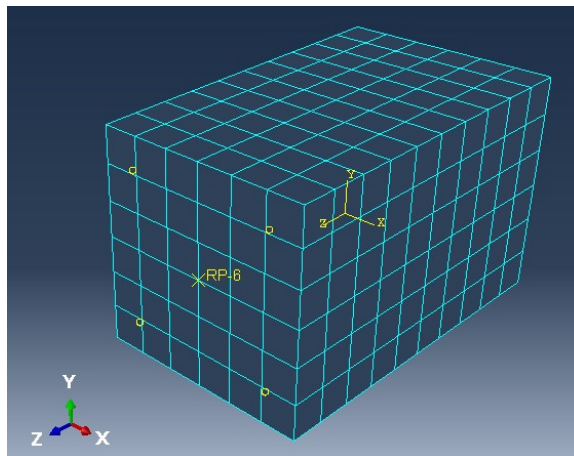


Figure 5.2. Meshed column in ABAQUS.

5.3 Boundary Condition and Loading

All the modelled columns in ABAQUS were fixed in the bottom in all directions and released in the top except the top middle point where the load was applied as shown in Figure 5.3. In order

to obtain the load-deflection behavior of the modelled columns, a static monotonic load was placed on the mid-top of the column. The loading was applied until failure using the displacement control technique. Displacement increments were adjusted to 3mm in each step.

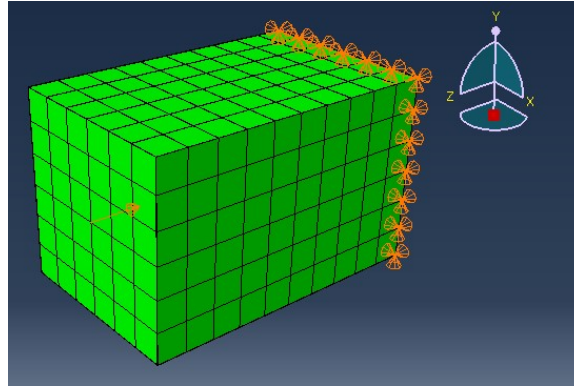


Figure 5.3. Boundary condition and loading in ABAQUS.

5.4 Description of Material Model and Properties

5.4.1 Concrete

The elastic performance of concrete was determined based on the elastic modulus and Poisson's ratio. The values of those parameters were used as specified in the experimental data. For the inelastic behavior, ABAQUS uses the concrete damage plasticity (CDP) constitutive model. This model considers two main failure mechanisms, which are tensile cracking and compressive crushing [ABAQUS \(2008\)](#).

The CDP model in ABAQUS forms from plastic behavior, compressive behavior, and tensile behavior. The compressive behavior of concrete requires determining the relationship between the yield stress and inelastic strain. The CDP model is primary developed for reinforced concrete structures. Thus, a design-oriented stress-strain model for concrete [Lam & Teng \(2003b\)](#) was implemented.

Plastic Behavior of Concrete

To define the plasticity model of concrete, there are some fundamental parameters which need to be defined. Those parameters are the dilation angle (ψ), the plastic potential eccentricity (e), the ratio of initial equibiaxial compressive yield stress to initial uniaxial compressive yield stress (f_{b_o}/f_{c_o}), the ratio of the second stress invariant on the tensile meridian which controls the shape of the yield surface (K_c), and the viscosity (u). The dilation angle was used as 31 based on calibration. The eccentricity e , (f_{b_o}/f_{c_o}), k_c , and u were defined as 0.1, 1.16, 2/3, and zero respectively [Demir et al. \(2016\)](#).

Compressive Behavior of Concrete

To obtain the compressive behavior for confined concrete with FRP, a design-oriented stress-strain model is used [Lam & Teng \(2003b\)](#). The first part of the stress-strain curve is a parabolic line and the second part is a straight line as shown in Figure 5.4. The slope of the parabola line is the modulus of elasticity of the unconfined concrete. The parabolic line meets the straight line smoothly so there is no change in slope between the two portions. For simplicity, the intersection point of the two lines represents the unconfined compressive strength f'_{co} . The stress-strain curve ends at a point where both the ultimate compressive strength f'_{cc} and the ultimate axial strain ϵ_{cu} of the confined concrete are reached.

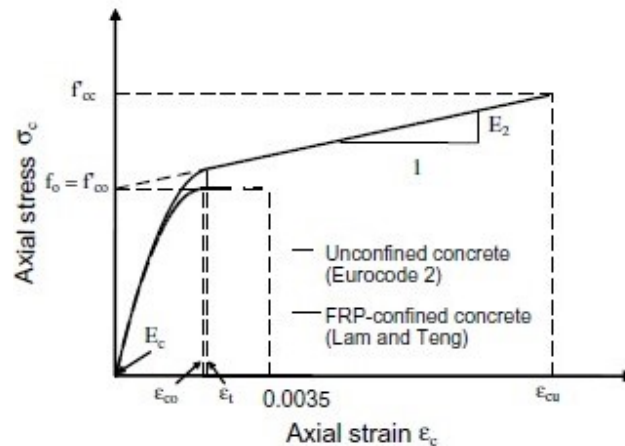


Figure 5.4. Lam and Teng's stress-strain model for FRP-confined concrete [Lam & Teng \(2003b\)](#).

The Lam and Teng stress-strain model for confined concrete is given by the following equations
Lam & Teng (2003b):

$$\sigma_c \begin{cases} E_c \varepsilon_c - \frac{(E_c - E_2)^2}{4f'_{co}} \varepsilon_c^2 & 0 \leq \varepsilon_c \leq \varepsilon_t \\ f'_{co} + E_c \varepsilon_c & \varepsilon_t \leq \varepsilon_c \leq \varepsilon_{cu} \end{cases} \quad (71)$$

where:

$$\varepsilon_t = \frac{2f'_{co}}{E_c - E_2} \quad (72)$$

$$\varepsilon_t = \frac{f'_{cc} - f'_{co}}{\varepsilon_{cu}} \quad (73)$$

In which σ_c is the axial stress, ε_c is the axial strain of confined concrete, E_c is the elastic modulus of unconfined concrete, ε_t is the axial strain at the transition point, and E_2 is the slope of the straight line of the curve.

In this model f'_{cc} is obtained from Samaan et al. (1998):

$$\frac{f'_{cc}}{f'_{co}} = 1 + k_1 \frac{f_l}{f'_{co}} \quad (74)$$

where f_l is the confining pressure and it can be obtained from:

$$f_l = \frac{2\sigma_j t}{d} = \frac{2E_{frp}\varepsilon_j t}{d} \quad (75)$$

In which σ_j is the FRP jacket hoop stress, t is the total thickness of FRP, d is the diameter of the confined concrete core, E_{frp} is the FRP modulus of elasticity in hoop direction, and ε_j is the hoop tensile strain of the FRP at failure. The hoop stress σ_j is related to the hoop strain ε_j and it can be obtained from Equation (76) as applied in the confining pressure formula:

$$\sigma_j = E_{frp}\varepsilon_j \quad (76)$$

In the developing confinement model, it has been suggested that the hoop tensile strain ε_j should be taken as the actual hoop rupture strain measured in the FRP jacket $\varepsilon_{h,rupt}$ ($\varepsilon_j = \varepsilon_{h,rupt}$) rather than considering it as FRP material ultimate tensile strain ε_{rup} as existed in most of the FRP confined concrete models [Karbhari & Gao \(1997\)](#) [Saafi et al. \(1999\)](#) [Pessiki et al. \(2001\)](#). Also, the value of k_1 in Equation (74) is considered as 3.3 [Lam & Teng \(2003b\)](#).

FRP efficiency factor K_ε has been proposed to relate the actual hoop rupture strain $\varepsilon_{h,rupt}$ to the FRP material ultimate tensile strain ε_{rup} [Pessiki et al. \(2001\)](#):

$$\varepsilon_{rup} = K_\varepsilon \varepsilon_{frp} \quad (77)$$

It has been shown that the value of the efficiency factor K_ε is varying with the type of the FRP. Based on database collected from the literature, it has been found that the average value of K_ε is 0.586 for carbon FRP (CFRP) [Lam & Teng \(2003a\)](#).

To calculate the ultimate axial strain of uniformly confined concrete ε_{cu} , the following equation is used:

$$\frac{\varepsilon_{cu}}{\varepsilon_{co}} = 1.75 + k_2 \frac{f_l}{f'_{co}} \left(\frac{\varepsilon_{h,rupt}}{\varepsilon_{co}} \right)^{0.45} \quad (78)$$

In which ε_{co} is the axial strain at the compressive strength of unconfined concrete, and k_2 is the strain enhancement coefficient. The value of those two parameters is 0.002 and 12 respectively [Lam & Teng \(2003a\)](#).

This design- oriented stress-strain model was extended to model rectangular concrete columns confined with FRP. Therefore, some modifications were applied to the compressive strength and ultimate axial strain formulas by adding shape factors k_{s1} and k_{s2} as shown below:

$$\frac{f'_{cc}}{f'_{co}} = 1 + k_1 k_{s1} \frac{f_l}{f'_{co}} \quad (79)$$

$$\frac{\varepsilon_{cu}}{\varepsilon_{co}} = 1.75 + k_2 k_{s2} \frac{f_l}{f'_{co}} \left(\frac{\varepsilon_{h,rupt}}{\varepsilon_{co}} \right)^{0.45} \quad (80)$$

Those shape factors are proposed to take into consideration the effective confined concrete area in rectangular columns since the rectangular sections have non-uniform confinement stress. The strength enhancement k_{s1} and the strain enhancement k_{s2} shape factors are defined as follow [Lam & Teng \(2003b\)](#):

$$k_{s1} = \left(\frac{b}{h}\right)^\alpha \frac{A_e}{A_c} \quad (81)$$

$$k_{s2} = \left(\frac{h}{b}\right)^\beta \frac{A_e}{A_c} \quad (82)$$

where $h \geq b$, and A_e/A_c is the effective confinement area ratio. Based on some experimental data, the value of the two exponents α and β have been found to be 2 and 0.5 respectively [Lam & Teng \(2003b\)](#).

5.4.2 Reinforcement

The behavior of steel was modelled as elastic perfectly plastic model. The parameters which were used to define the model are modulus of elasticity, yield stress, and Poisson's ratio. Figure 5.5 illustrates the reinforcement arrangement for BS2 in ABAQUS.

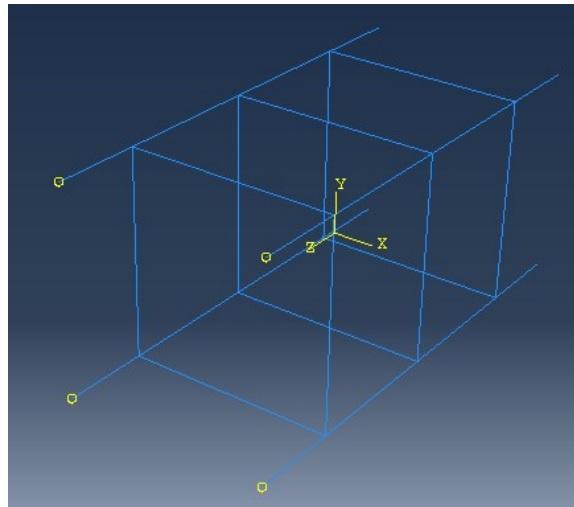


Figure 5.5. Reinforcement configuration in ABAQUS for BS2.

5.4.3 FRP

FRP is considered in ABAQUS as unidirectional lamina composites. A unidirectional lamina is considered as a homogenous body and consisting of continuous fibres strongly bonded in a matrix as shown in Figure 5.6. The longitudinal fibres are the load-carrying elements while the matrix provides protection to the fibres and distributes the load between fibres [Cristescu et al. \(2003\)](#). The FRP jacket is modelled as linear elastic orthotropic material, which means that the mechanical

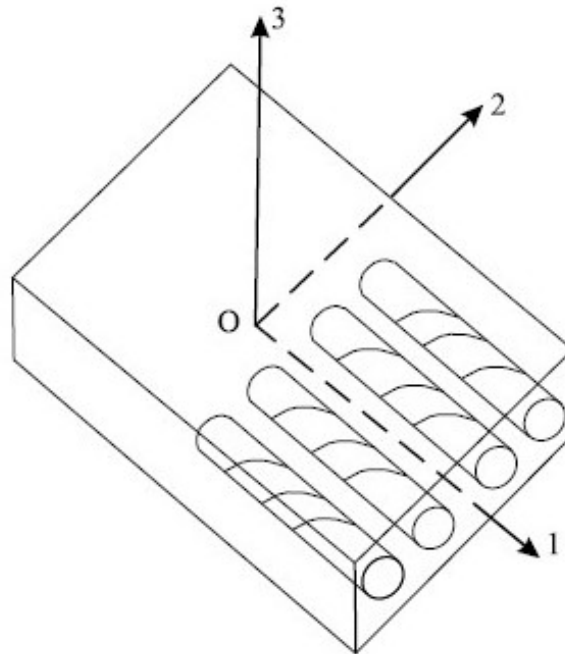


Figure 5.6. Lamina with unidirectional fibres [Cristescu et al. \(2003\)](#).

properties of the material are inconsistent in different directions.

To determine the composite in-plane elastic properties which are required for FRP in ABAQUS (Figure 5.7), the ‘mechanics of material approach’ is used. This approach assumes that the composite is void-free, the fibres have the same shape and size, they are distributed equally, and fibres are perfectly bonded to the matrix. Accordingly, the overall properties of the composite are obtained based on volume fractions for both fibres (f) and matrix (m).

Longitudinal Young modulus E_1 is estimated based on the rule of mixtures by assuming the

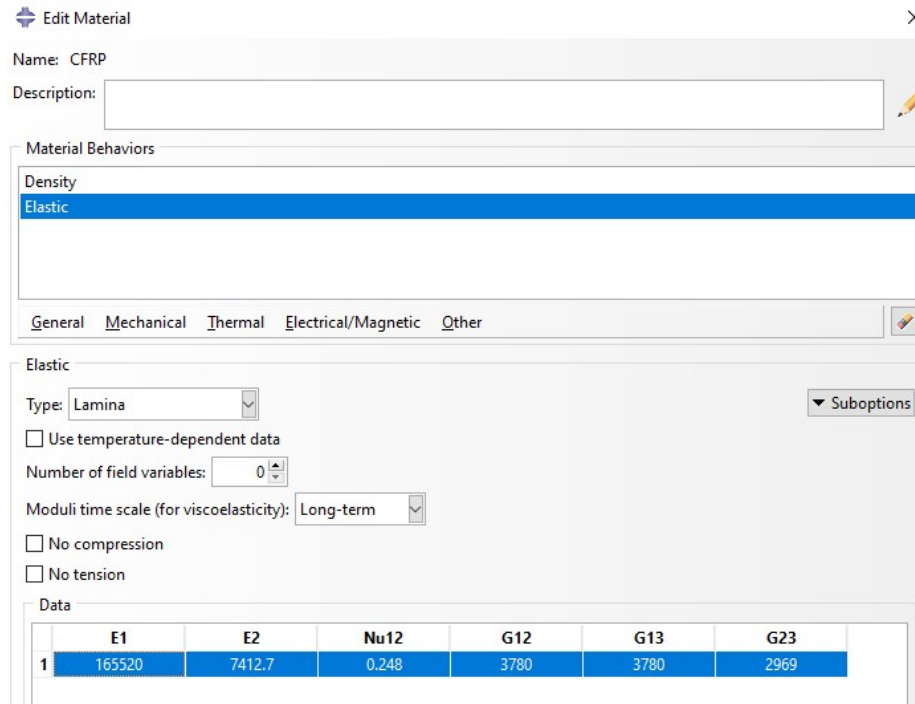


Figure 5.7. Material properties required for FRP in ABAQUS.

same strain in the fibre and matrix [Kollar & Springer \(2003\)](#) as follows:

$$E_1 = E_m V_m + E_f V_f \quad (83)$$

whereas, the transverse Young modulus E_2 is determined from the following relation that is often called the inverse rule of mixtures:

$$\frac{1}{E_2} = \frac{V_m}{E_m} + \frac{V_f}{E_f} \quad (84)$$

The overall Poisson's ratio ν_{12} can be obtained by using the same assumption of the rule of mixtures as follows:

$$\nu_{12} = \nu_m V_m + \nu_f V_f \quad (85)$$

where V_m is the volume fraction of the matrix, V_f is the volume fraction of the fibre, E_m and E_f are the Young moduli for the matrix and fibre respectively. The rest of the Poisson's ratios in the

different directions are determined by using Maxwell relation [Tsai \(1988\)](#) as given below:

$$\frac{v_{ij}}{E_i} = \frac{v_{ji}}{E_j} \quad (86)$$

Since the composite material is subjected to shear stress, shear moduli are required for modeling transverse shear deformation in all directions. The overall in-plane shear modulus G_{12} can be estimated by assuming that the fibre and matrix have the same shear stress [Cristescu et al. \(2003\)](#). Thus, the shear modulus of the composite material is calculated from the following:

$$\frac{1}{G_{12}} = \frac{V_m}{G_m} + \frac{V_f}{G_{f12}} \quad (87)$$

where G_m and G_f are the shear moduli for the matrix and fibre respectively. The subscripts 1,2, and 3 represent the laminate coordinate system. Axis 1 is parallel to the fibres, axis 2 is perpendicular to the fibres, and axis 3 is perpendicular to the plain of Lumina as illustrated in [Figure 5.6](#).

Usually it is assumed that the unidirectional lamina can be treated as transversely isotropic material [Soden et al. \(2004\)](#). Accordingly, the independent elastic constants are minimized to five since $E_2 = E_3$, $G_{12} = G_{13}$, $v_{12} = v_{13}$ and $G_{23} = E_2/2(1 + v_{23})$ [Tsai \(1988\)](#).

The FRP sheets are modelled as lamina composites in ABAQUS. The mechanical properties of the composites are obtained from the experimental data [Rousakis & Karabinis \(2012\)](#).

Since there are not enough experimental data available about the composite's in-plane elastic properties, some reasonable assumptions were made based on the type of the FRP sheet for numerical modeling purposes. The carbon C-sheet 240 is made from carbon fibres and epoxy resins as a matrix to support the fibres. The mechanical properties for the carbon fibres and the resin epoxy matrix that were considered in the ABAQUS modeling [Daniel et al. \(2006\)](#) are shown in [Table 5.1](#) and [Table 5.2](#).

To obtain the mechanical properties of the unidirectional lamina that are entered in ABAQUS software, the rule of mixtures is used as explained in the equations above. Regarding the volume fractions of both fibres and matrix, two assumptions were made. The assumptions are; the ratio between $E_f/E_m = 30$ and the matrix volume fraction is 0.3, accordingly the fiber volume fraction is 0.7 [Matthys \(2000\)](#).

Table 5.1. Mechanical properties of the carbon fiber.

Property	Carbon fibre (AS4)
Density (g/cm^3)	1.81
Longitudinal modulus, E_{f1} (GPa)	235
Transverse modulus, E_{f2} (GPa)	15
Axial shear modulus, G_{f12} (GPa)	27
Transverse shear modulus, G_{f21} (GPa)	7
Poisson's ratio ν_{f12}	0.2

Table 5.2. Mechanical properties of the resin epoxy matrix.

Property	Epoxy matrix (HY6010)
Density (g/cm^3)	1.17
Young's modulus, E_m (GPa)	3.4
Shear modulus G_m (GPa)	1.26
Poisson's ratio ν_m	0.36

Table 5.3 illustrates the mechanical properties of the lamina composites based on; the mechanical properties of the fibres and matrix, assumptions that were made, and the equations that were derived based on the rule of mixture.

Table 5.3. The mechanical properties of the lamina composites as used in ABAQUS.

Property	E_1 (GPa)	E_2 (GPa)	ν_{12}	G_{12} (GPa)	G_{13} (GPa)	G_{23} (GPa)
CFRP	165.52	7.4127	0.248	3.78	3.78	2.969

Chapter 6

Numerical Results

6.1 Introduction

In this chapter, the outcomes of the 3D material model and the finite element model in ABAQUS are presented. All the results are graphically illustrated in terms of stress-strain curves. The results are obtained by converting the load-deflection curves into stress-strain curves. The vertical axis represents the stress which is calculated by dividing the load by the column's cross-section area. While the horizontal axis represents the strain which is computed by dividing the displacement by the length of the column. Each figure has three lines, those lines are representing the behavior of the concrete columns obtained from experiments, the 3D material model, and the ABAQUS software respectively.

6.2 Validation of the Numerical Model

The 3D material model was validated against the experimental results which are obtained from a previous study and another numerical finite element model that is generated by ABAQUS.

6.2.1 Reinforced Concrete Column

Figure 6.1 shows the performance of a reinforced concrete (RC) column with longitudinal and transverse steel bars. It is clear from the figure that the results of the 3D material model are in good

agreement with the experimental and the finite element model in ABAQUS. Therefore, this model has the ability to simulate the mechanical behavior of reinforced concrete columns.

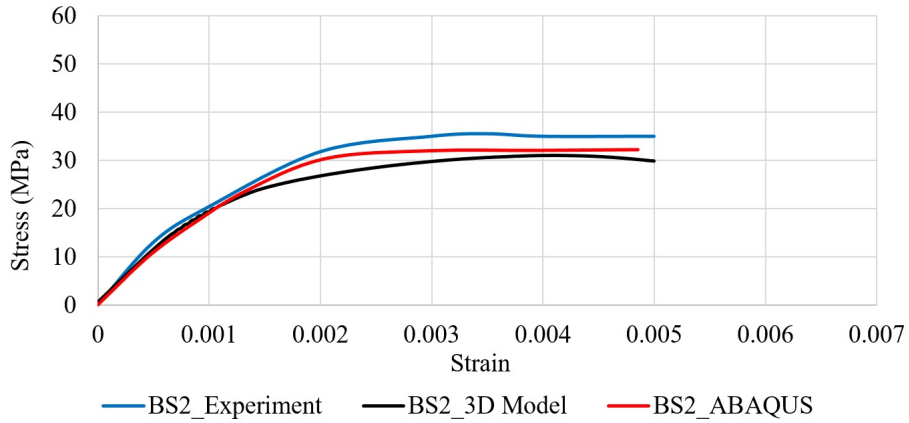


Figure 6.1. Stress-strain curve for reinforced concrete column (BS2).

6.2.2 Plain Concrete Columns Confined with FRP

Figures 6.2 and 6.3 illustrate the stress-strain curves for plain concrete columns confined with one and five carbon FRP layers respectively. The performance of the columns based on the 3D material model is in good harmony with the experimental and ABAQUS results. Therefore, the model can simulate the performance of confined concrete columns with different numbers of FRP layers.

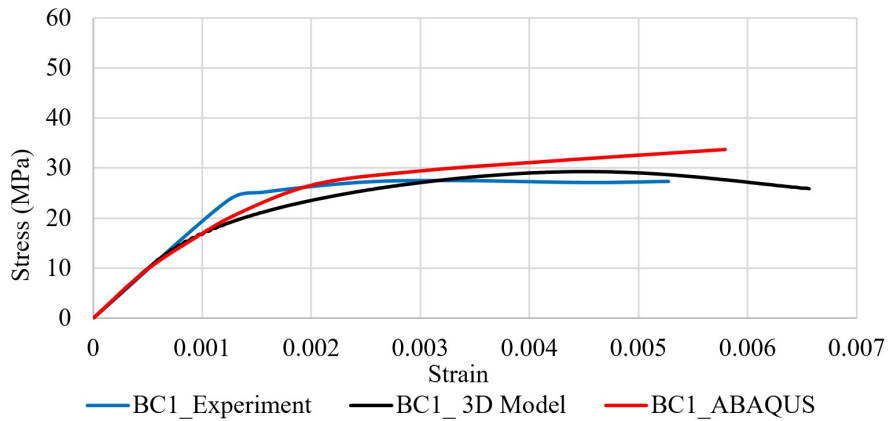


Figure 6.2. Stress-strain curve for plain concrete column wrapped with one FRP layer (BC1).

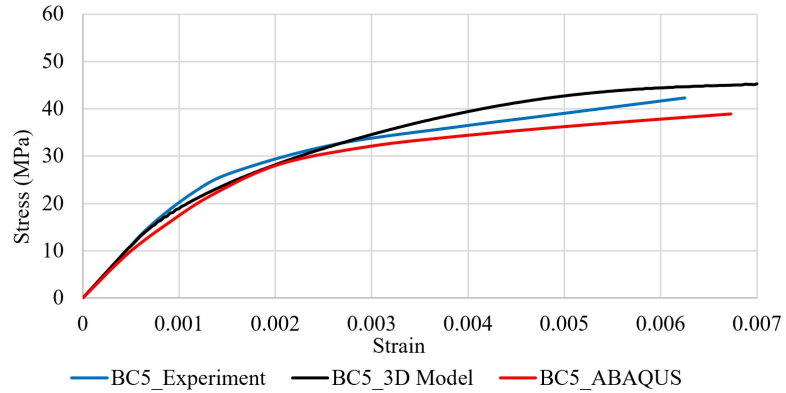


Figure 6.3. Stress-strain curve for plain concrete column wrapped with five FRP layers (BC5).

6.2.3 Reinforced Concrete Columns Confined with FRP

Figures 6.4-6.8 show the stress-strain curves at mid-span for retrofitted reinforced concrete columns with FRP. The model was tested for five different reinforced concrete column types; the reinforcement configuration and the number of FRP layers were different in each case. It is clear from the figures that the 3D numerical model can capture the behavior of reinforced concrete columns after FRP retrofitting since its performance is in good agreement with the experiment and ABAQUS outcomes.

Any difference between the results that are obtained from the 3D material model and ABAQUS could be due to using different material models for concrete and different finite element types. For example, to model the reinforcement in the 3D material model, a beam element was used while in ABAQUS, a truss element was used.

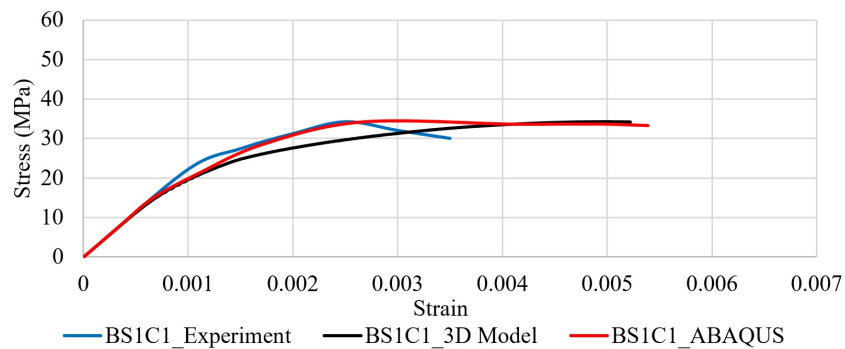


Figure 6.4. Stress-strain curve for RC column wrapped with one layer of FRP (BS1C1).

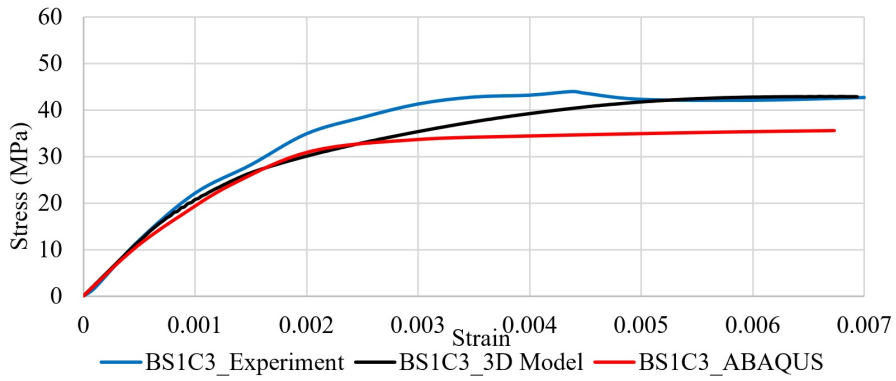


Figure 6.5. Stress-strain curve for RC column wrapped with three layers of FRP (BS1C3).

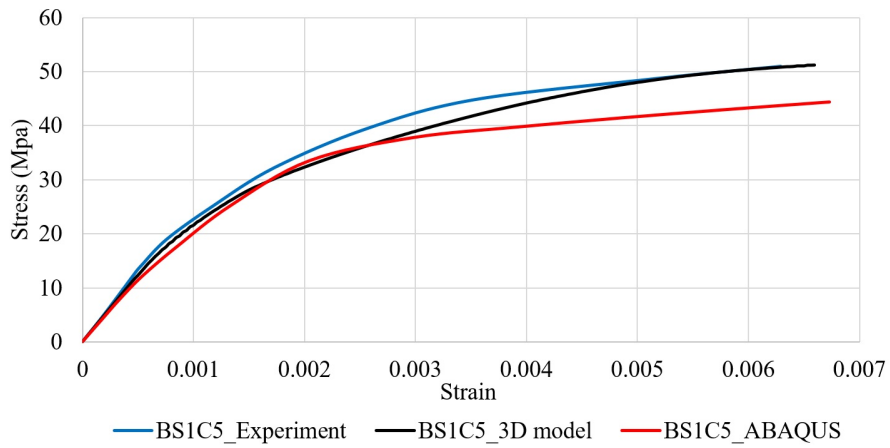


Figure 6.6. Stress-strain curve for RC column wrapped with five layers of FRP (BS1C5).

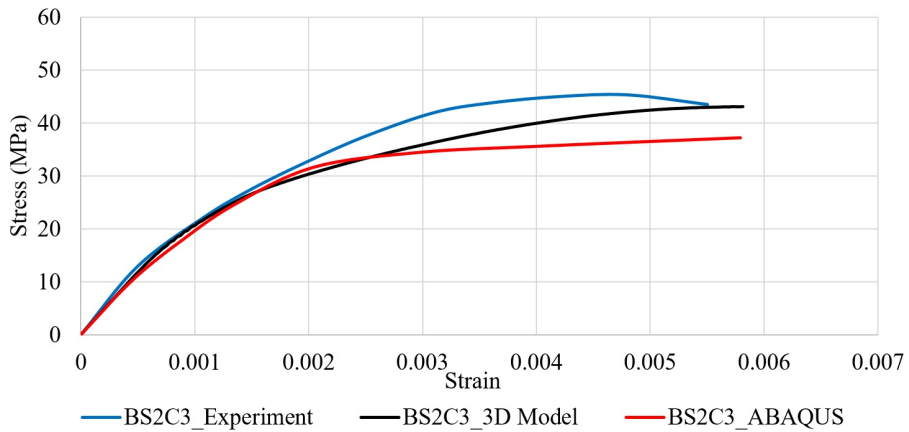


Figure 6.7. Stress-strain curve for RC column wrapped with three layers of FRP (BS2C3).

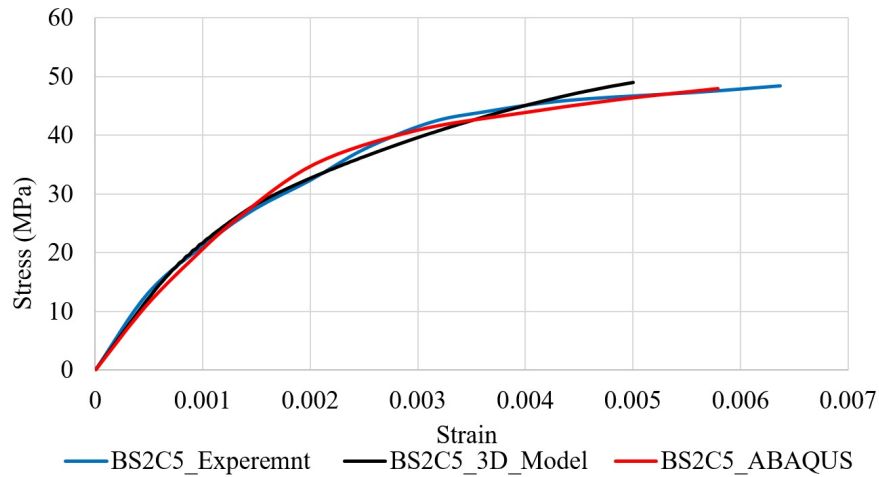


Figure 6.8. Stress-strain curve for RC column wrapped with five layers of FRP (BS2C5).

6.3 Results of the 3D Material Model

In order to compare the behavior of confined and unconfined concrete columns, the validated 3D material model was used. Figure 6.9 demonstrates the mechanical behavior of three different column types; unconfined column, confined columns with FRP jackets, and reinforced columns with FRP jackets. It is clear from the results that the load-carrying capacity of the columns increased when applying the FRP jackets. In addition, there is a direct relationship between the strength of the column and the number of applied FRP layers; the strength is increasing with the increase of the thickness of the FRP jacket (number of layers).

The enhancement in the column strength was 15% when applying one layer of the FRP and 80.7% when using five FRP layers. Applying reinforcement and one layer of FRP improved the load-carrying capacity of the column by approximately 9 MPa. The maximum increase in the axial stress of the column was reached when applying reinforcement and five layers of FRP to the unconfined column, the strength was almost doubled.

Furthermore, as observed from the results, the confined columns with FRP layers show more ductile behavior when compared with the unconfined case. The ductility can be remarked by the increase in the axial confined strain.

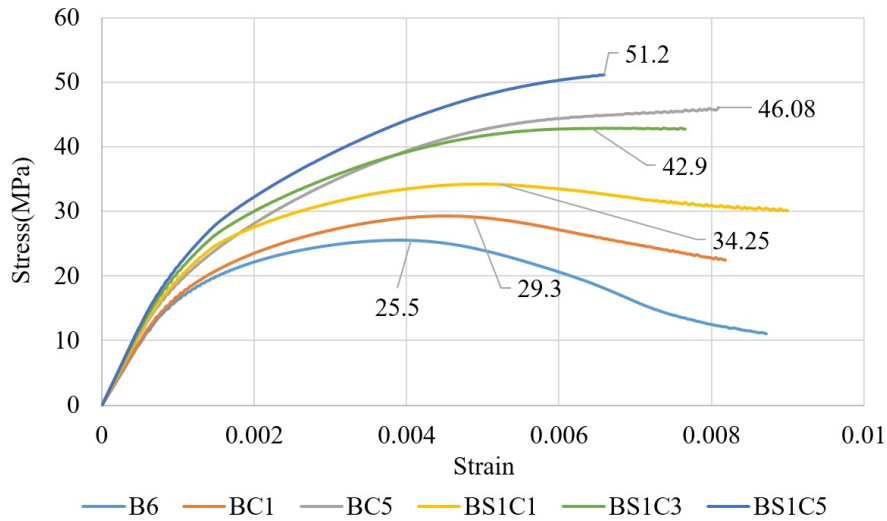


Figure 6.9. Stress-strain curves for retrofitted concrete columns using the 3D material model.

6.4 Parametric Study

A parametric study was conducted to test the sensitivity of the mesh size on the stress-strain curve of a confined reinforced concrete column with five layers of FRP using the 3D material model. In Figure 6.10, the numerical results of the stress-strain curve for BS2C5 are illustrated with mesh sizes of 64mm, 53mm, 40mm, and 32mm. It is clear from the results, that the mesh size does not have a major effect on the behavior of the retrofitted column when using the 3D material model.

In addition, the 3D material model was used to model partially wrapped plain concrete (BC1) and reinforced concrete (BS2C5) columns. Their behavior was compared with fully and unwrapped (unconfined) cases as shown in Figure 6.11 and Figure 6.12 respectively. The width of the FRP layer was 32 mm and the vertical spacing of the FRP strips was 32mm which started from the bottom of the column. Another spacing distance of 96mm was used in the case of the plain concrete column. The FRP strips configuration is graphically demonstrated in Figure 6.13 for 32 mm and 96mm vertical spacing. It was concluded that the 3D model is capable of modeling partially wrapped columns. It is obvious from the outcomes that the partial wrapping technique can enhance the strength of the columns. In addition, it was noticed that when FRP strips spacing decreases, the load-carrying capacity of the column rises.

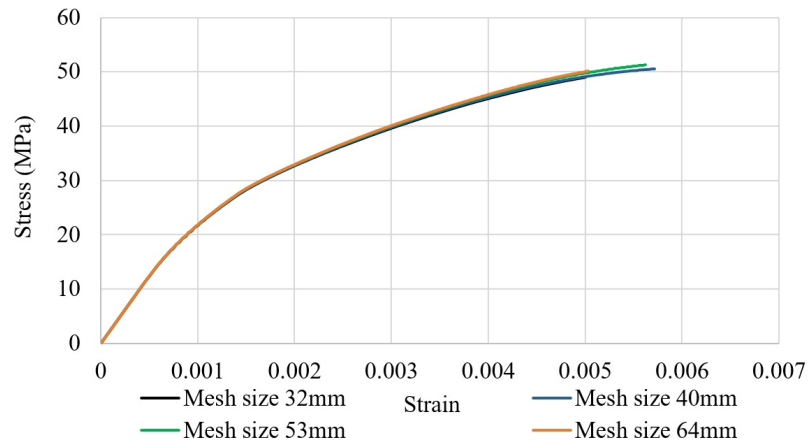


Figure 6.10. Stress-strain curve for BS2C5 with different mesh sizes using 3D material model.

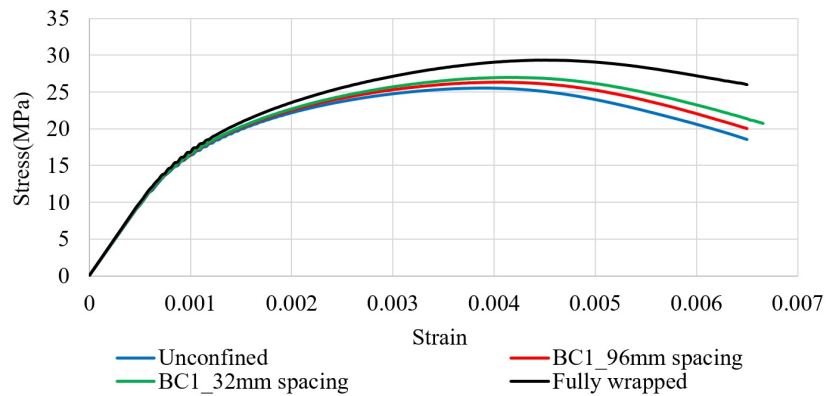


Figure 6.11. Comparing the behavior of partially wrapped plain concrete column (BC1) with different spacing with fully wrapped and not wrapped cases using 3D material model.

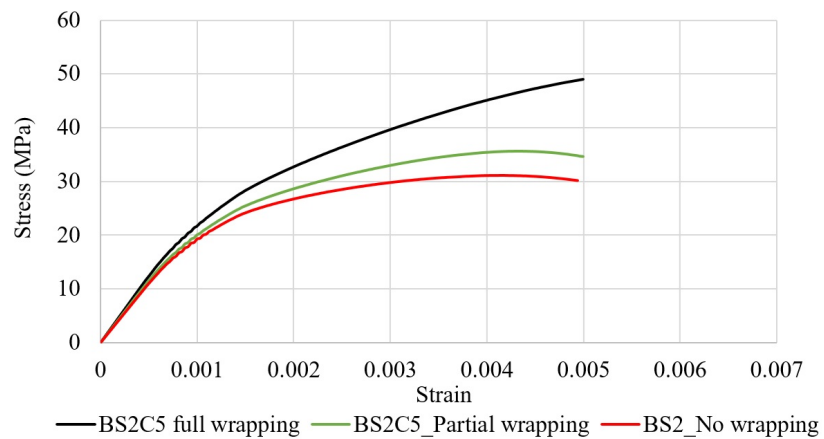
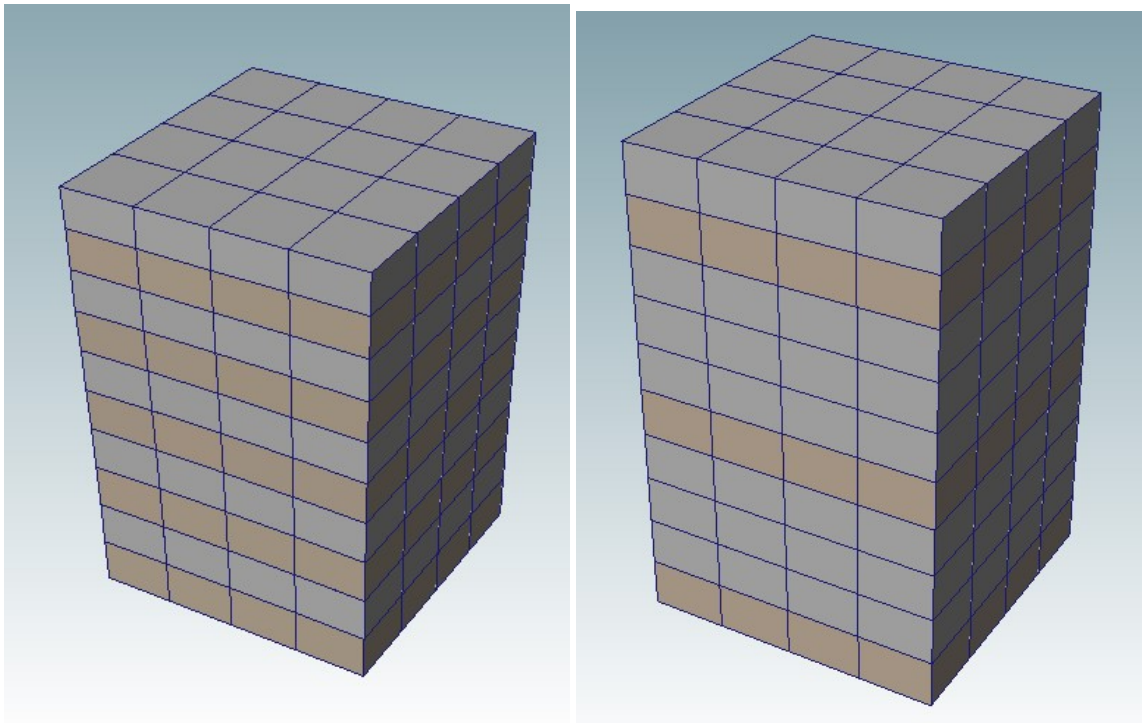


Figure 6.12. Comparing the behavior of partially wrapped reinforced concrete column (BS2C5) with fully wrapped and not wrapped cases using 3D material model.



(a) 32mm spacing.

(b) 96mm spacing.

Figure 6.13. Different vertical spacing of FRP strips on the concrete column.

Chapter 7

Implementation of Optimization Method to Obtain the Confined Strain Equation

7.1 Introduction

Using building design codes is very important to ensure adequate structural safety and quality. Engineers depend on the design codes and standards to provide guidance and minimum requirements for sufficiently designed elements. Recently, many countries and institutions have established codes, guidance, and standards for designing confined reinforced concrete columns with FRP.

For example, the American Concrete Institute (ACI 440.2R,2017) has introduced a section with four pages length for designing confined concrete columns with FRP, the German Committee for Structural Concrete (DAfStb- Guideline, 2012) has a section with five pages length, and the Standardization Administration of the People's Republic of China (GB 50608, 2010) has considered the design of confined concrete columns with a section of eight pages in length. Whereas, the Canadian Standards Association (CSA S806, 2012) is limited to one-page length. The number of pages reveals the significance of considering the confinement effect in several standards.

This chapter presents an optimization method procedure that is recommended to the Canadian Standards with respect to the maximum confined concrete strain. A design formula is proposed to describe the effect of the concrete and FRP mechanical parameters on the value of strain. To obtain this effect numerically, a parametric study is conducted using the 3D material model. The

data involved in this parametric study are used to define the designed formula with the aid of the optimization algorithm, performing what is known as nonlinear regression.

7.2 Gaps and Limitations in the Canadian Standards

While reviewing and comparing the above codes, it has been found that the Canadian Standards (CSA S806-12) has gaps and limitations in designing confined reinforced concrete columns with FRP as summarized below:

- CSA S806-12 is limited to fully wrapped columns only so there is no consideration for partially wrapped columns.
- CSA S806-12 is not providing a formula to calculate the maximum confined concrete strain after applying FRP. It always considers the confined strain as the peak concrete strain value which is 0.0035. However, an accurate value for confined concrete strain is important to predict the behavior of confined columns under axial compressive load.
- CSA S806-12 does not specify any design model for the confined concrete.
- When wrapping rectangular columns, the code is limited to a ratio of 1.5 to h/b ($h/b \leq 1.5$).
- For rectangular sections confined with transverse FRP laminates, section corners shall be rounded to a radius not less than 20 mm before the FRP application.
- CSA S806-12 is limited to the ultimate limit state so there is no consideration for serviceability limit state.
- The load combination that considered in CSA S806-12 is a combination of axial compression and bending (not applicable for axial compression only)
- CSA S806-12 considers a strength reduction factor of 0.75 for FRP jackets without considering the type of composite material (e.g. Carbon FRP or Glass FRP).

7.3 Discussing the Gaps and Limitations in the Canadian Standards

The current work is focusing on presenting recommendations to fill some of the gaps and limitations in the Canadian Standards that are related to the design of concrete columns reinforced with FRP composites. In this chapter, a parametric study is conducted using the 3D material model in order to provide a design formula for the maximum confined concrete strain that is wrapped with FRP layers using nonlinear regression.

The outcomes of the 3D material model show that the model has the ability to model partially wrapped columns as illustrated in section 6.4 while the Canadian Standards is limited to fully wrapped columns only. The load capacity of the column increases when the spacing of the FRP strips decreases. Also, the results of the 3D model show that the maximum confined concrete strain is increasing with the number of applied FRP layers (Figure 7.1) not as specified in the CSA S806-12 as a fixed value, which is equal to the peak concrete strain 0.0035.

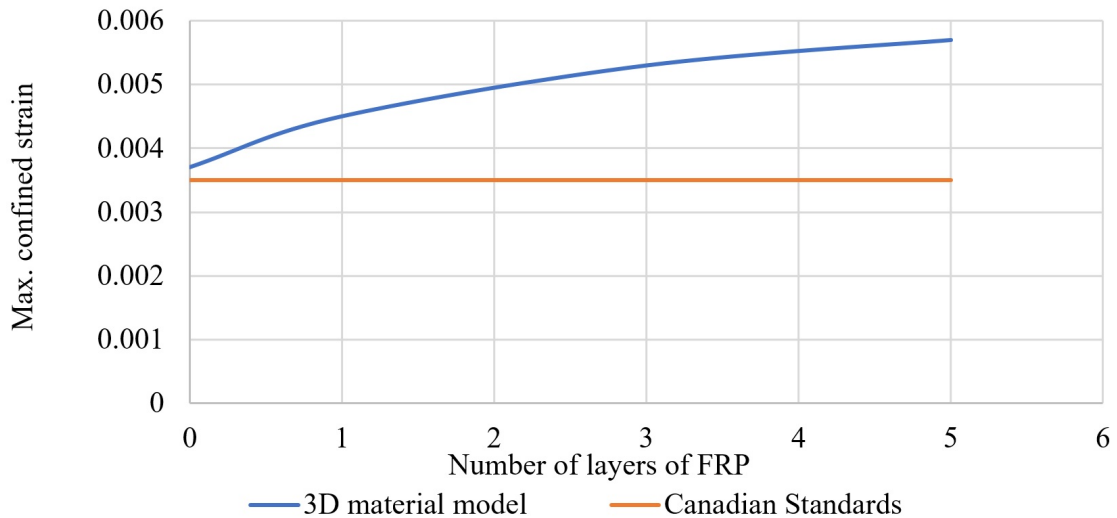


Figure 7.1. Maximum confined concrete strain vs number of layers of FRP from 3D material model and the Canadian Standards.

Figure 7.2 shows the stress-strain curves of the unconfined plain concrete column and the performance of the column when adding different numbers of FRP layers. It is clear from the results that there is a direct relationship between the number of applied FRP jackets and the maximum confined concrete strain value. Moreover, the same relationship is applied for the reinforced concrete column

as demonstrated in Figure 7.3. The maximum confined strain increased from 0.0042 to 0.0073 after adding five layers of FRP to the reinforced concrete column. Accordingly, the effect of the FRP layers (confinement effect) on the maximum confined concrete strain should be addressed clearly.

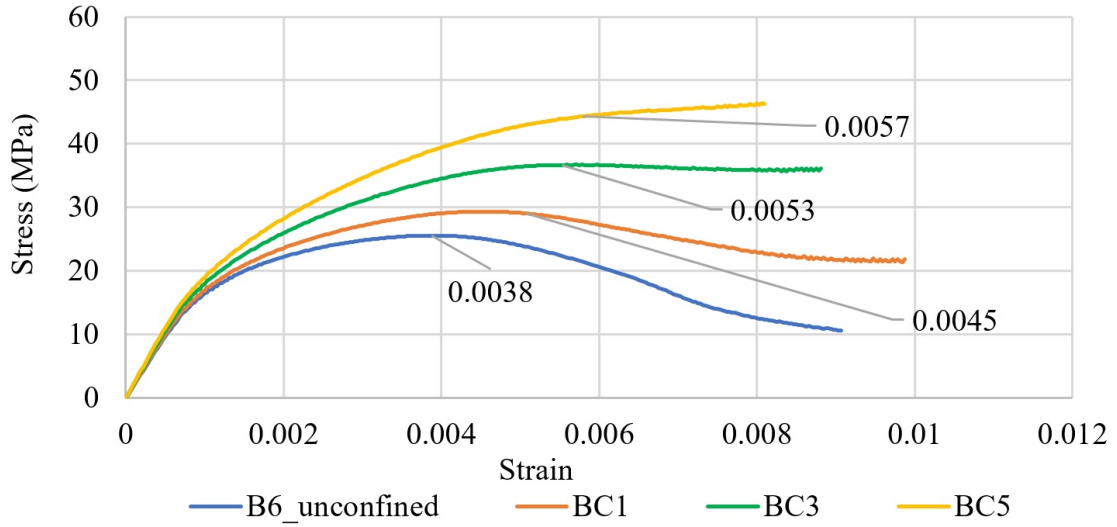


Figure 7.2. Stress-strain curves for plain concrete column wrapped with different number of FRP layers using the 3D material model.

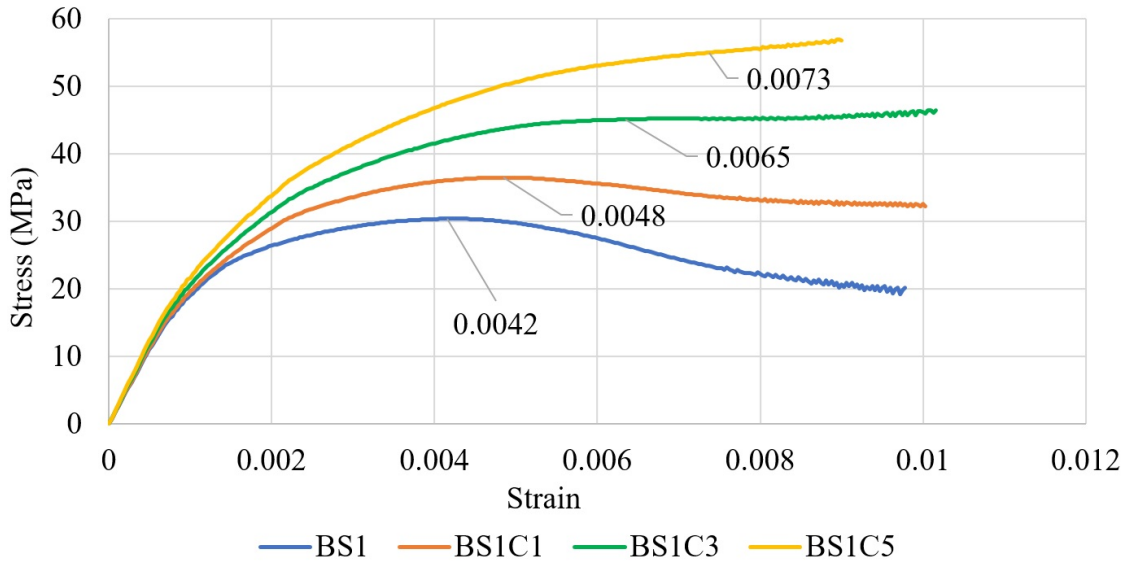


Figure 7.3. Stress-strain curves for reinforced concrete column wrapped with different number of FRP layers using the 3D material model.

The ACI 440.2R-17 considered the effect of the applied FRP layers to the concrete columns on the maximum concrete strain (ε_{cc}) as specified in the following equation:

$$\varepsilon_{cc} = \varepsilon_{c0}k_2 + \varepsilon_{c0}k_3 \frac{f_{lj}}{f_c} \left(\frac{\varepsilon_{ju}}{\varepsilon_{c0}} \right)^{k_4} \quad (88)$$

where f_c is the unconfined concrete strength, ε_{c0} is the peak unconfined concrete strain, ε_{ju} is the FRP's rupture strain, f_{lj} is the confinement pressure provided by FRP as shown in Equation (89), and $k_2 - k_4$ are factors with values of 1.5, 12, and 0.45 respectively.

$$f_{lj} = \frac{2t_j E_j \varepsilon_{ju}}{D} \quad (89)$$

where t_j is the thickness of the FRP, E_j is the modulus of the composite material, and D is the diameter of the circular cross-section.

The Chinese guidance (GB 50608, 2010) used the following approach for finding the confined concrete strain:

$$\varepsilon_{cc} = 0.0035 + 0.015 \sqrt{\frac{f_{ljd}}{f_{cd}}}, \quad f_{ljd} \leq 0.6 \varepsilon_{FRP,k} \quad (90)$$

where f_{ljd} is the design FRP jacket strength, f_{cd} is the design concrete strength, and $\varepsilon_{FRP,k}$ is the characteristic maximum strain for an FRP sheet.

The German standards (DAfStb- Guideline, 2012) implemented the same approach as used in the ACI 440.2R-17 but with different factors and $\frac{f_{lj}}{f_c}$ was replaced by $\frac{f_{ljk}}{f_c}$. In which f_{ljk} is the characteristic FRP jacket strength, and $k_2 - k_4$ are 1.75, 19, and 0 respectively.

7.4 The Proposed Nonlinear Regression Algorithm to Obtain the Maximum Confined Concrete Strain

In this part of the work a nonlinear regression is performed, where data obtained from a parametric study is fit to a model and then expressed as a mathematical function. The nonlinear regression method is illustrated in Algorithm 1. This method starts by defining the **Inputs** which are:

- Geometry parameters of the column include: the dimensions of the column, boundary conditions, and mesh sizing.
- Material parameters which are: concrete unconfined strength, concrete modulus of elasticity, concrete Poisson's ratio, unconfined concrete strain, the thickness of the FRP layer, tensile and shear modulus of FRP layer and the Poisson's ratio of FRP.
- A combination of thirteen possible equations for the maximum confined concrete strain for square columns under compressive load.

Algorithm 1: The Nonlinear Regression Algorithm

Input : Geometry parameters, Material parameters , Possible Equations
Output: Regression parameters

- 1 Set the inputs for the tested column in the 3D material model program ;
- 2 Set the parametric study using structural analysis program ;
- 3 Run the structural analysis program ;
- 4 Obtain the output data in tabulated format ;
- 5 Load selected parameters (from **Step 2**) and the maximum confined strain and strength (from **Step 4**) into the Matlab code ;
- 6 Set possible number of \mathcal{N} equation forms for the maximum confined concrete strain ;
- 7 **for** $i \leftarrow 1$ to \mathcal{N} **do**
- 8 Define a set of initial conditions (\mathcal{M}) for the parameter coefficients related to Equation i ;
- 9 Run the optimization code to obtain the optimal parameter coefficients for initial condition of Equation i ;
- 10 Select regression parameters that correspond to the best performance ;
- 11 **end**
- 12 Compare the performance of the \mathcal{N} equations ;
- 13 Rank the \mathcal{N} equations ;
- 14 Return regression parameters of the best equation

The terms of the equations were suggested based on the literature and design standards reviewing [Ozbakkaloglu et al. \(2013\)](#). There are unlimited numbers of equations that can be recommended to be tested by the optimization procedure. In the current research, thirteen equations for calculating the maximum confined concrete strain under compressive load were recommended to be fitted to the 3D material model results as shown below:

$$Eq_1 : \varepsilon'_{cc} = k_1 + \frac{k_2 + \log(t_{frp}) * E_{frp}^{\varepsilon_{ju}}}{(b * f_c)^{k_3}} + k_4 * \log\left(\frac{E_{conc}}{f'_{cc}}\right) \quad (91)$$

$$\mathbf{Eq}_2 : \varepsilon'_{cc} = k_1 + \frac{k_2 + \log(t_{frp}) * E_{frp}^{\varepsilon_{ju}}}{(b * f_c)^{k_3}} \quad (92)$$

$$\mathbf{Eq}_3 : \varepsilon'_{cc} = k_1 + \frac{k_2 + \log(t_{frp}) * E_{frp}^{\varepsilon_{ju}}}{(b * f_c)} + k_3 * \log\left(\frac{E_{conc}}{f'_{cc}}\right) \quad (93)$$

$$\mathbf{Eq}_4 : \varepsilon'_{cc} = k_1 + \frac{k_2 + \log(t_{frp}) * E_{frp}^{\varepsilon_{ju}}}{(b * f_c)} + k_3 * \log\left(\frac{E_{conc} * \varepsilon_{ju}}{f'_{cc}}\right) \quad (94)$$

$$\mathbf{Eq}_5 : \varepsilon'_{cc} = k_1 + k_2 * \log(t_{frp}) + k_3 * \log\left(\frac{E_{conc}}{f'_{cc}}\right) \quad (95)$$

$$\mathbf{Eq}_6 : \varepsilon'_{cc} = k_1 + k_2 * t_{frp} + k_3 * \frac{E_{conc}}{f'_{cc}} \quad (96)$$

$$\mathbf{Eq}_7 : \varepsilon'_{cc} = k_1 + \left(\frac{k_2 * t_{frp} * E_{frp}}{b * f_c}\right)^{k_3} \quad (97)$$

$$\mathbf{Eq}_8 : \varepsilon'_{cc} = (k_1 * \frac{t_{frp} * E_{frp}}{b * f_c})^{k_2} + k_3 * \frac{f_c}{f'_{cc}} \quad (98)$$

$$\mathbf{Eq}_9 : \varepsilon'_{cc} = k_1 + k_2 * t_{frp} + k_3 * \left(\frac{E_{frp} * f_c}{E_{conc} * f'_{cc}}\right) \quad (99)$$

$$\mathbf{Eq}_{10} : \varepsilon'_{cc} = k_1 + k_2 * t_{frp} + k_3 * \left(\frac{E_{frp} * \log(f_c)}{E_{conc} * f'_{cc}}\right) \quad (100)$$

$$\mathbf{Eq}_{11} : \varepsilon'_{cc} = k_1 + k_2 * t_{frp} + k_3 * \left(\frac{E_{frp} * \log(f_c)}{E_{conc} * \log(f'_{cc})}\right) \quad (101)$$

$$\mathbf{Eq}_{12} : \varepsilon'_{cc} = k_1 + (k_2 * \frac{k_3 + k_4 * \log(t_{frp}) * E_{frp}^{\varepsilon_{ju}}}{k_5 * b * f_c})^{k_6} \quad (102)$$

$$Eq_{13} : \varepsilon'_{cc} = 0.0035 * k_1 + 0.0035 * k_2 \left(\frac{2 * t_{frp} * E_{frp} * \varepsilon_{ju}}{b * f_c} \right) \left(\frac{\varepsilon_{ju}}{0.0035} \right)^{k_3} \quad (103)$$

The steps for the nonlinear regression algorithm are as follows:

- **Step 1:** Is to **Set** the inputs for the 3D material model. These inputs are the column geometry and the material parameters.
- **Step 2:** In order to **Set** the parametric study, a structural analysis program that is written on the FORTRAN Language is used. This program is working in parallel with the 3D material model based on changing some material parameters simultaneously in the model's input folders as shown in the given example in Figure (7.4) to test their effect on the maximum confined concrete strain. The parameters that were alternating are the thickness of the FRP layer, unconfined concrete strength, the elastic modulus of concrete, and the tensile modulus of FRP.
- **Step 3:** **Run** the structural analysis program.
- **Step 4:** **Obtaining** the corresponding maximum confined concrete strain and strength from the outputs and tabulated in Table 7.1.
- **Step 5:** **Load** the thickness of FRP layer t_{frp} , unconfined concrete strength f_c , elastic modulus of concrete E_{conc} , tensile modulus of FRP E_{frp} , confined concrete strength f'_{cc} , the rupture strain of the FRP ε_{ju} , and width of the column cross-section b into the **Matlab** code.
- **Step 6:** **Set** the possible number of equations (Equation 91 - 103) in the **Matlab** code.
- **Step 7- Step 8:** **Define** a set of initial values for the parameter coefficients related to each equation.
- **Step 9:** **Run** the optimization code to obtain the optimal parameter coefficients for the Equations. The optimization method used in this work is based on least squares optimization algorithm and it is illustrated in *fitnlm* (n.d.), which was developed by MathWorks developers. The method proved its efficiency and reliability to perform linear and nonlinear regression. The Matlab function $mdl = fitnlm(tbl, modelfun, beta0)$ is used to fit the model specified

by *modelfun* to variables in the table or dataset array *tbl*, and returns the nonlinear model *mdl*. then, *fitnlm* estimates model coefficients using an iterative procedure starting from the initial values in *beta0*. The term *tbl* represents the material parameters and the corresponding confined concrete strain and strength shown in Table 7.1. The term *modelfun* represents the possible equations. The term *beta0* is the initial values for the coefficient in the proposed equation.

- **Step 10:** The optimization method calculates the R^2 value, P-value, and Mean Square Error for tuned coefficient, and then **Select** regression parameters that correspond to the best performance.
- **Step 12- Step 13: Compare and Rank** the equations based on their performance.
- **Step 14: Return** regression parameters of the best equation.

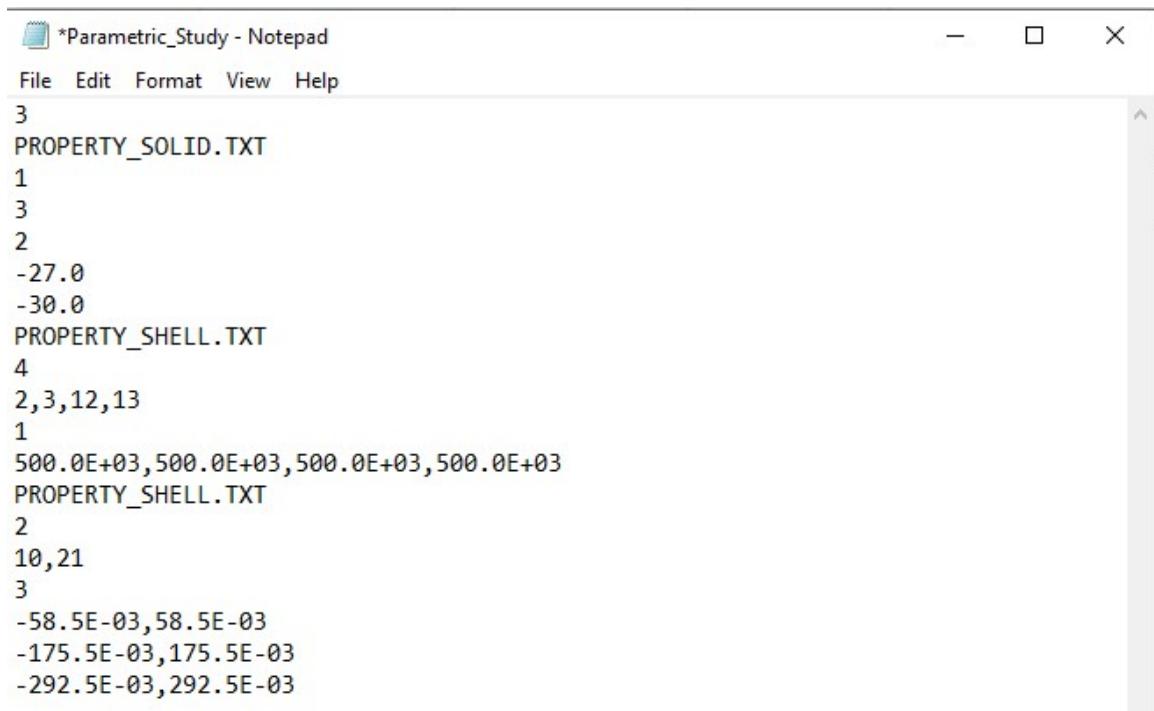


Figure 7.4. Changing some of the material parameters simultaneously in the structural analysis program.

Table 7.1. The material parameters and the corresponding confined concrete strain and strength.

		Parameter 1	Parameter 2	Parameter 3	Parameter 4	Parameter 5
	ε_{cc}	t_{frp} (mm)	f_c (MPa)	E_{conc} (MPa)	E_{frp} (MPa)	f'_{cc} (MPa)
1	0.0044	0.117	-25.5	19300	240000	29.33
2	0.00534	0.351	-25.5	19300	240000	36.61
3	0.00578	0.585	-25.5	19300	240000	44.31
4	0.00618	0.785	-25.5	19300	240000	51.2625
5	0.0043	0.117	-25.5	20000	240000	29.23
6	0.0052	0.351	-25.5	20000	240000	36.38
7	0.0059	0.585	-25.5	20000	240000	44.22
8	0.00625	0.785	-25.5	20000	240000	51.12
9	0.00418	0.117	-25.5	20500	240000	29.175
10	0.00512	0.351	-25.5	20500	240000	36.209
11	0.0058	0.585	-25.5	20500	240000	44.05
12	0.006188	0.785	-25.5	20500	240000	50.85
13	0.00415	0.117	-25.5	21500	240000	29.078
14	0.005125	0.351	-25.5	21500	240000	35.925
15	0.00575	0.585	-25.5	21500	240000	43.624
16	0.00625	0.785	-25.5	21500	240000	50.68
17	0.00378	0.117	-25.5	23000	240000	28.9
18	0.0048	0.351	-25.5	23000	240000	35.523
19	0.00525	0.585	-25.5	23000	240000	42.635
20	0.00581	0.785	-25.5	23000	240000	49.587
21	0.0044	0.117	-25.5	19300	220000	29.036
22	0.0052	0.351	-25.5	19300	220000	35.692
23	0.0057	0.585	-25.5	19300	220000	42.809
24	0.00625	0.785	-25.5	19300	220000	49.306
25	0.0044	0.117	-25.5	19300	260000	29.629
26	0.00556	0.351	-25.5	19300	260000	37.608
27	0.006125	0.585	-25.5	19300	260000	46.298
28	0.0045	0.117	-25.5	19300	280000	29.925
29	0.00556	0.351	-25.5	19300	280000	38.535
30	0.00625	0.585	-25.5	19300	280000	47.998
31	0.00453	0.117	-25.5	19300	300000	30.219
32	0.00575	0.351	-25.5	19300	300000	39.534

The material parameters and the corresponding confined concrete strain and strength (**Continue**).

		Parameter 1	Parameter 2	Parameter 3	Parameter 4	Parameter 5
	ε_{cc}	t_{frp} (mm)	f_c (MPa)	E_{conc} (MPa)	E_{frp} (MPa)	f'_{cc} (MPa)
33	0.00625	0.585	-25.5	19300	300000	49.49
34	0.0035	0.117	-20	19300	240000	23.096
35	0.00434	0.351	-20	19300	240000	28.917
36	0.004656	0.585	-20	19300	240000	35.105
37	0.00515	0.785	-20	19300	240000	41.007
38	0.00518	0.117	-30	19300	240000	34.422
39	0.00625	0.351	-30	19300	240000	42.915
40	0.0044375	0.117	-25.5	19500	240000	29.3123
41	0.00475	0.117	-27	19300	240000	31.039
42	0.005	0.117	-29	19300	240000	33.3036
43	0.0054	0.117	-31	19300	240000	35.566
44	0.0035	0.117	-20	19300	220000	22.86
45	0.00431	0.117	-25	19300	220000	28.472
46	0.005156	0.117	-30	19300	220000	34.077
47	0.003531	0.117	-20	19300	260000	23.33
48	0.00437	0.117	-25	19300	260000	29.05
49	0.00522	0.117	-30	19300	260000	34.766
50	0.0036	0.117	-20	19300	300000	23.8
51	0.00444	0.117	-25	19300	300000	29.63
52	0.00531	0.117	-30	19300	300000	35.46
53	0.00475	0.117	-27	19300	240000	31.04
54	0.005109	0.117	-29	19300	240000	33.3
55	0.0054	0.117	-31	19300	240000	35.56
56	0.00418	0.351	-20	19300	220000	28.148
57	0.00528	0.351	-25	19300	220000	35.028
58	0.00593	0.351	-30	19300	220000	41.74
59	0.00428	0.351	-20	19300	260000	29.605
60	0.00544	0.351	-25	19300	260000	36.882
61	0.0043	0.351	-20	19300	300000	31.04
62	0.00547	0.351	-25	19300	300000	38.69
63	0.00509	0.117	-27	19300	500000	34.94
64	0.005625	0.117	-30	19300	500000	38.74

7.4.1 Performance Measures

In this work P- values, R^2 , Mean Square Error (MSE) and graphical analysis of the data set are used to identify whether the used equations with their optimal coefficients are suitable to express the relation between maximum strain and material properties.

P-value is a conditional probability that identifies whether the obtained results are significant or not when the null hypothesis is assumed to be true. The null hypothesis is a hypothesis that is used in statistics to show that there is no difference between certain specified populations. For example, there is no statically significant relationship between the type of food I feed the cows and the growth of the cows. In other words, the coefficients in the equation are not important, there is no significant effect. The alternative hypothesis is the opposite of the null hypothesis which means that there is a difference between two or more variables. For example, the coefficients in the equation are important and have a significant effect. When the p-value is less than a chosen significant level then the null hypothesis is rejected. This significant level is type 1 error (α) which is the probability of rejecting the null hypothesis when it is true and usually it specified as 0.05. The test hypothesis is characterized as below:

H_0 (Null hypothesis): $\beta_i = 0$ [coefficient is not important]

H_1 (Alternative hypothesis): $\beta_i \neq 0$ [coefficient is important]

The R-squared (R^2) or the coefficient of determination is a statistical measure of how close the data are to the fitted regression line. While the Mean Squared Error (MSE) measures the average of the squares of the error that indicates how close the regression line is to the set of points. The graphical analysis of the data set is illustrated in the next subsection.

7.4.2 Results and Discussion

The results from the nonlinear regression are represented as:

- The R^2 value, coefficient optimal parameters, and P-values for each equation as shown in Table 7.2.
- The maximum strain obtained from the 3D material model vs maximum strain obtained from each equation is graphically illustrated in Figure 7.5 to Figure 7.17. The black dots indicate

the material model strain obtained from the parametric study using the 3D material model, while the red dots represent the fitted strain from each proposed equation.

- The Mean Square Error for all proposed equations as demonstrated in Figure 7.18

After comparing the outcomes of the proposed algorithm, it was shown that there are three equations provided the best fitting, these equations are:

- Eq_1 which has the maximum coefficient of determination value of 0.979, and minimum MSE value of $1.35e-08$ and the P-values for the four optimal coefficients are less than 0.05, which means that all the coefficients are significant to Eq_1 . The graphical analysis of the data set for this equation that is shown in Figure 7.5 demonstrates an accurate fitting to the material model strain data set.
- Eq_5 has a coefficient of determination value of 0.957, MSE of $2.66e-08$, and all its parameter coefficients are significant. Figure 7.9 shows that this equation provides a suitable fitting to the data set.
- Eq_6 has a coefficient of determination value of 0.956 and MSE of $2.72e-08$. Based on the P-values, this equation has three coefficients, only two of them are significant to the equation. Figure 7.10 shows that this proposed equation demonstrates a good fitting to the material maximum strain.

The equations that showed the worst fitting are:

- Eq_7 which has a low coefficient of determination value of 0.378, and the higher MSE of $3.88e-07$. The P-values demonstrate that only one of its coefficients is significant to the equation. Figure 7.11 shows that this equation has a bad fitting to the material model strain data set.
- Eq_{10} which also has a low coefficient of determination value of 0.491 and a high MSE of $3.18e-08$. The graphical analysis of the data set for this equation in Figure 7.14 confirms this assessment.

- Eq_{13} has the lowest coefficient of determination with the value of 0.374 and a high MSE of $3.84e - 07$. Figure 7.17 reveals the worst fitting among all equations.

Table 7.2. The results obtained from nonlinear regression algorithm with respect to each possible equation.

Equation#	Initial values	R2	Optimal parameters	P-value	MSE
Eq.1	12 0.01 0.5 70	0.979	k1=0.024818 k2=-51.879 k3 =1.1999 k4=-0.0029206	4.6966e-33 0.00022232 7.961e-40 5.4989e-23	1.35e-08
Eq.2	1 120 0.5	0.892	k1=0.0091448 k2=-24.77 k3=1.005	5.2125e-41 4.248e-14 4.183e-83	6.71e-08
Eq.3	0.003 0.01 7	0.889	k1=0.011276 k2=-21.836 k3=-0.00036508	7.1299e-17 3.6696e-14 0.032744	6.30e-08
Eq.4	0.003 0.01 -7	0.889	k1=0.010595 k2=-21.836 k3=-0.00036508	1.0062e-22 3.6696e-14 0.032744	6.30e-08
Eq.5	0.003 12 7	0.957	k1= 0.030397 k2 =0.00012541 k3 =-0.0040304	1.4556e-40 0.0040699 4.4035e-35	2.66e-08
Eq.6	0.003 12 7	0.956	k1=0.0090297 k2=-0.00023872 k3=-6.7948e-06	1.6775e-50 0.077188 1.4235e-34	2.72e-08
Eq.7	0.003 12 7	0.378	k1 =0.0041323 k2 =4.2841e-06 k3=0.68949	1.3381e-06 0.89377 0.25234	3.88e-07
Eq.8	0.1 2.7 1.2	0.733	k1 =0.021655 k2 = -0.13069 k3 =-0.015856	1.5444e-16 1.4786e-21 9.1023e-14	1.67e-07
Eq.9	0.003 12 0.2	0.517	k1=0.0032483 k2= 0.0030953 k3= 8.5339e-05	1.5131e-08 8.2621e-09 0.030504	3.01e-07
Eq.10	1 1.2 1	0.491	k1=0.0049043 k2=0.0018967 k3=-0.00037153	3.9461e-14 0.00010302 0.23275	3.18e-07
Eq.11	1 12 1	0.527	k1=0.003337 k2=0.0026876 k3=7.235e-05	2.6166e-11 2.7188e-11 0.015174	2.95e-07
Eq.12	0.0035 1 2 3 12 0.5	0.669	k1 = -0.4033 k2=-0.097571 k3=-0.19835 k4=-1.6628e+05 k5=79027 k6=0.2263	6.6333e-11 0.99112 0.97342 0 0 0.97386	2.06e-07
Eq.13	1.5 12 0.45	0.374	k1=1.2577 k2=0.078382 k3= -0.56192	1.1434e-40 1.1178e-08 1.9197e-82	3.84e-07

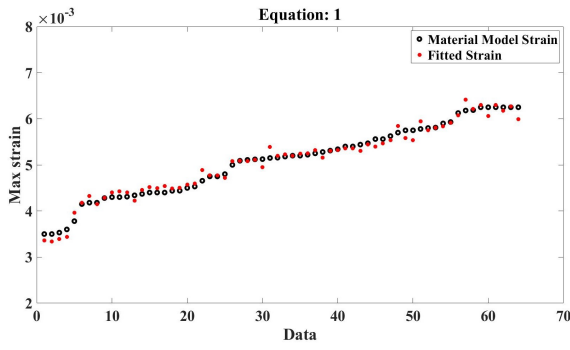


Figure 7.5. Maximum strain obtained from 3D material model vs maximum strain obtained from Equation 1.

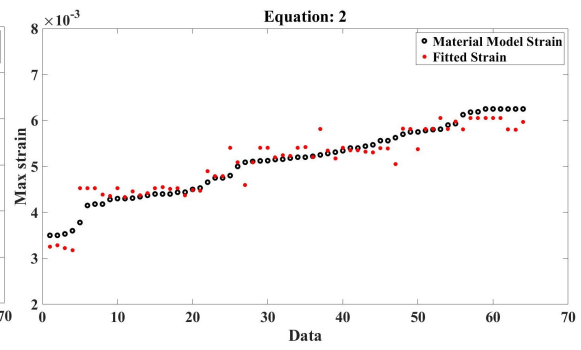


Figure 7.6. Maximum strain obtained from 3D material model vs maximum strain obtained from Equation 2.

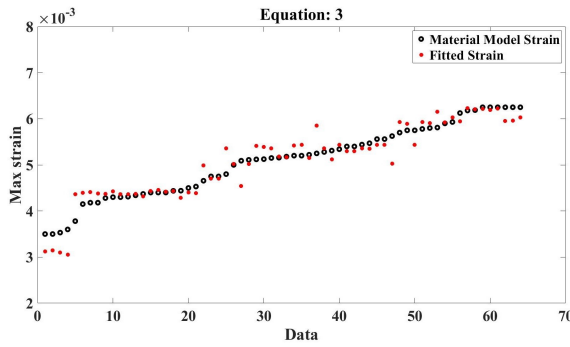


Figure 7.7. Maximum strain obtained from 3D material model vs maximum strain obtained from Equation 3.

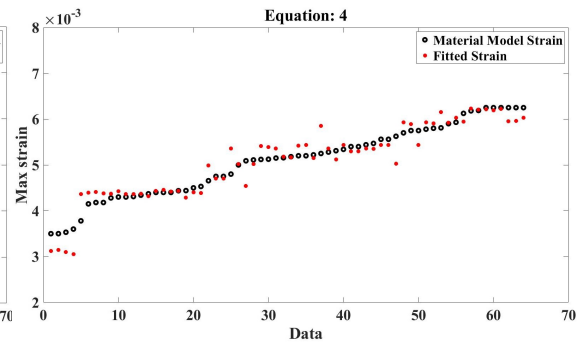


Figure 7.8. Maximum strain obtained from 3D material model vs maximum strain obtained from Equation 4.

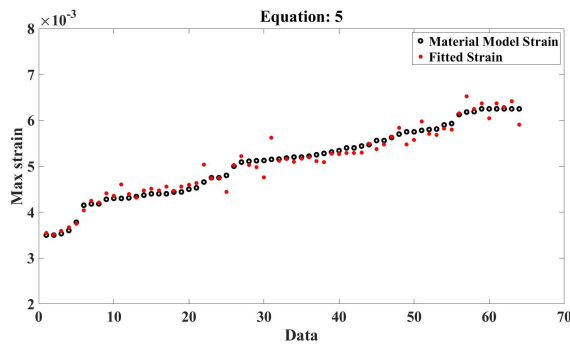


Figure 7.9. Maximum strain obtained from 3D material model vs maximum strain obtained from Equation 5.

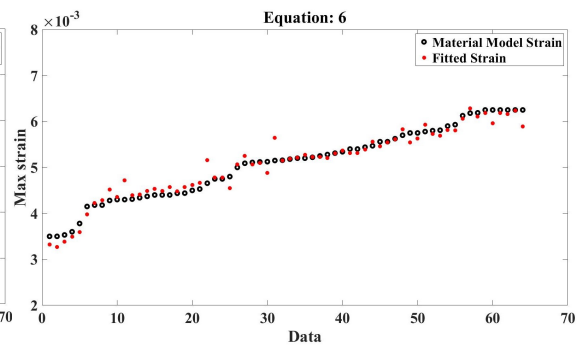


Figure 7.10. Maximum strain obtained from 3D material model vs maximum strain obtained from Equation 6.

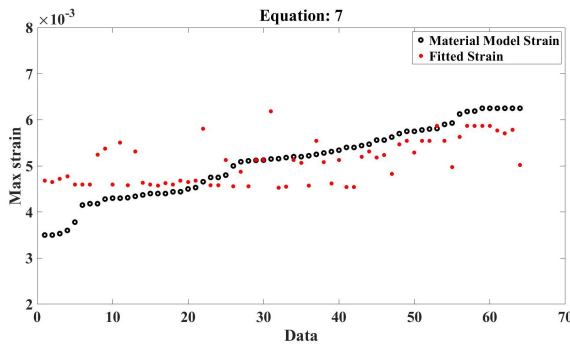


Figure 7.11. Maximum strain obtained from 3D material model vs maximum strain obtained from Equation 7.

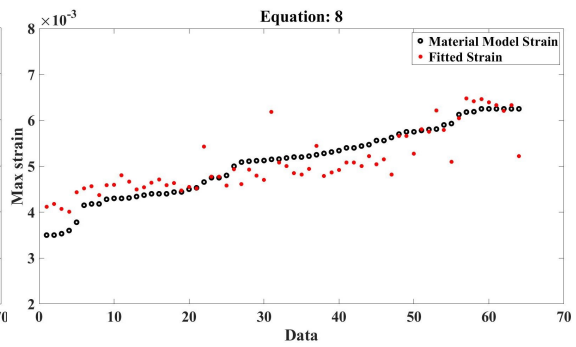


Figure 7.12. Maximum strain obtained from 3D material model vs maximum strain obtained from Equation 8.

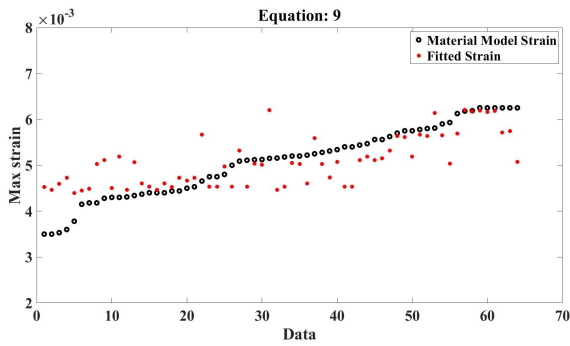


Figure 7.13. Maximum strain obtained from 3D material model vs maximum strain obtained from Equation 9.

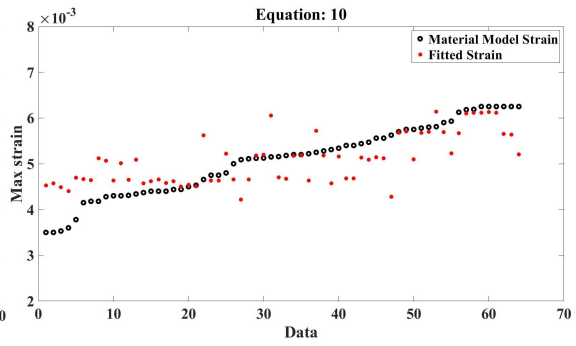


Figure 7.14. Maximum strain obtained from 3D material model vs maximum strain obtained from Equation 10.

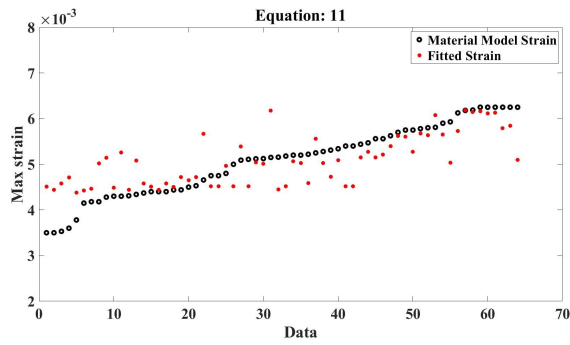


Figure 7.15. Maximum strain obtained from 3D material model vs maximum strain obtained from Equation 11.

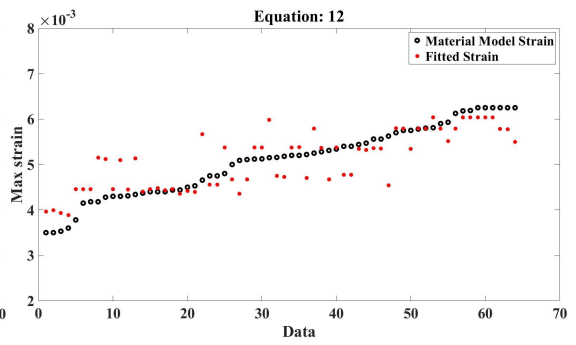


Figure 7.16. Maximum strain obtained from 3D material model vs maximum strain obtained from Equation 12.

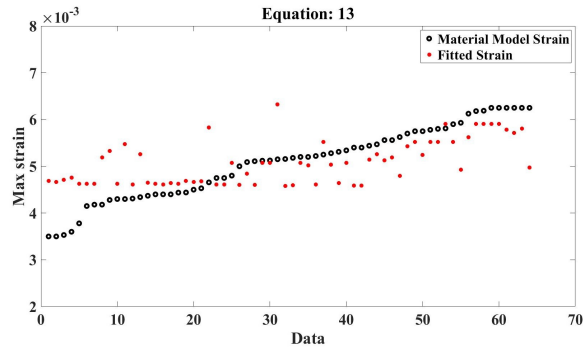


Figure 7.17. Maximum strain obtained from 3D material model vs maximum strain obtained from Equation 13.

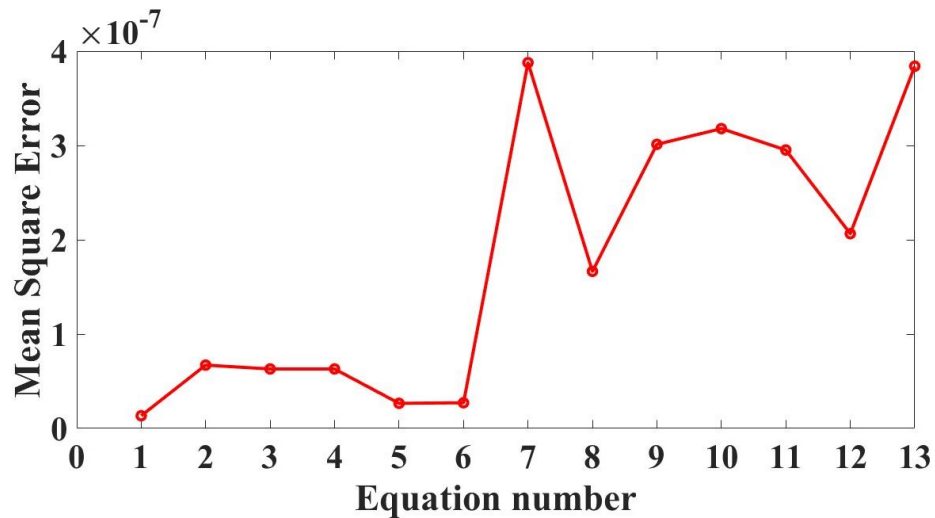


Figure 7.18. The Mean Square Error for all proposed equations.

7.5 Summary Outcome

An optimization-based nonlinear regression algorithm was proposed to test the performance of the proposed equations for the maximum confined concrete strain. The objective function of the optimization method that is performed in Matlab is to minimize the mismatch between the strain calculated from each equation (ε'_{cc}) and the obtained strain from the 3D material model (ε_{cc}).

Equation 13 was selected from the American standards (ACI 440.2R-17) to be tested in the nonlinear regression. The only change that was done is replacing the diameter D with the width of column b since the proposed equation in the ACI 440.2R-17 is for circular cross-section and in this work, the column's cross-section is squared. It has been found that the coefficients k_1 - k_3 in E_{q13}

are 1.257, 0.0078 and -0.562 respectively to perform best fitting to the 3D material model results. However, the values of those coefficient in ACI 440.2R-17 are as follows $k_1= 1.5$, $k_2= 12$, and $k_3= 0.45$.

Based on the performance measure of each equation, it has been shown that the following equations are providing the best fitting to maximum confined concrete strain that is obtained from the 3D material model:

$$\mathbf{Eq}_1 : \varepsilon'_{cc} = k_1 + \frac{k_2 + \log(t_{f_{rp}}) * E_{f_{rp}}^{\varepsilon_{ju}}}{(b * f_c)^{k_3}} + k_4 * \log\left(\frac{E_{conc}}{f'_{cc}}\right)$$

$$\mathbf{Eq}_5 : \varepsilon'_{cc} = k_1 + k_2 * \log(t_{f_{rp}}) + k_3 * \log\left(\frac{E_{conc}}{f'_{cc}}\right)$$

$$\mathbf{Eq}_6 : \varepsilon'_{cc} = k_1 + k_2 * t_{f_{rp}} + k_3 * \frac{E_{conc}}{f'_{cc}}$$

Chapter 8

Conclusion and Future Work

8.1 Introduction

This study is conducted to capture the behavior of retrofitted concrete columns with Fibre Reinforced Polymer (FRP). Given this, a 3D material model based on elasto-plastic models is adopted using the FORTRAN language. 3D elasto-plastic models are particularly suitable for the modeling and analysis of retrofitted concrete columns as confinement pressure is generally unknown before the analysis, which depends on the size, shape, loading, boundary conditions as well as material properties.

This research is mainly focused on the validation of a 3D elasto-plastic model. Accordingly, finite element analysis software ABAQUS is used to develop a numerical finite element model for the confined concrete columns. The parameters of the concrete constitutive model are introduced in detail in the 3D material model and in the ABAQUS model. Also, the same material properties and boundary conditions of the column are used in both models. The 3D material model is verified by comparing its outcome with the ABAQUS finite element model and experimental results from the literature.

A parametric study is generated to illustrate the applicability of the proposed 3D constitutive model in modeling partially wrapped square concrete columns and to test the effect of some material properties on the confined concrete strain. The outcomes of the parametric study are recommended to improve a part of the Canadian Standards which is related to concrete columns reinforced with

FRP composites. Consequently, a nonlinear regression algorithm is proposed to obtain an equation to calculate the maximum confined strain based on optimization method. This developed algorithm tested the performance of multiple equations and classified these equations based on their respective R^2 values, P-values, MSE, and graphical behavior.

8.2 Summary Discussion

The major findings and observations from this study are summarized as follows:

- The 3D material model was validated against the ABAQUS model and the experimental results in simulating the behavior of retrofitted columns with FRP composites under monotonic axial compressive loading.
- The proposed 3D material model has the ability to clearly predict the performance of fully and partially wrapped concrete square columns with FRP under compressive load.
- The FRP jacket which is applied to the concrete column increases the strength and the ductility of the column.
- The strength of partially wrapped square concrete columns rises as the FRP strips vertical spacing reduces.
- Mesh size does not have a significant effect on the column behavior when modeling the column using the 3D material model.
- The material properties of the concrete and FRP affect the value of the maximum confined strain.
- There is a direct relationship between the number of the FRP layers applied to confine the concrete column and the value of the maximum confined concrete strain.
- Thirteen possible equations for the maximum confined strain were proposed to be tested using a nonlinear regression; with the aid of the optimization method, only three equations were recommended for the Canadian standards based on the higher R^2 and least P-value and MSE.

8.3 Recommendations for Future Work

Based on the work done in this research, the following are recommended for future studies in the field of modeling retrofitted concrete columns with FRP:

- Test the 3D material model for cyclic loading.
- Propose equations to calculate the maximum confined strength and strain for partially wrapped columns using the proposed nonlinear optimization method.
- Utilizing artificial intelligence approach to perform the nonlinear regression.

References

- ABAQUS, I. (2008). *Abaqus analysis user's manual, version 6.8*. ABAQUS Providence, RI.
- Armero, F., & Oller, S. (2000). A general framework for continuum damage models. i. infinitesimal plastic damage models in stress space. *International Journal of Solids and Structures*, 37(48-50), 7409–7436.
- Attard, M., & Setunge, S. (1996). Stress-strain relationship of confined and unconfined concrete. *Materials Journal*, 93(5), 432–442.
- Bakis, C. E., Bank, L. C., Brown, V., Cosenza, E., Davalos, J., Lesko, J., ... Triantafillou, T. (2002). Fiber-reinforced polymer composites for construction—state-of-the-art review. *Journal of composites for construction*, 6(2), 73–87.
- Basalo, F. J. D. C., Matta, F., & Nanni, A. (2012). Fiber reinforced cement-based composite system for concrete confinement. *Construction and Building Materials*, 32, 55–65.
- Beer, F. P., & Johnston, E. (1992). *Mechanics of materials. new york7 mcgraw-hill*. Inc.
- Benallal, A., Billardon, R., & Doghri, I. (1988). An integration algorithm and the corresponding consistent tangent operator for fully coupled elastoplastic and damage equations. *Communications in Applied Numerical Methods*, 4(6), 731–740.
- Borja, R. I. (2013). *Plasticity: modeling & computation*. Springer Science & Business Media.
- Carrazedo, R., Mirmiran, A., & de Hanai, J. B. (2013). Plasticity based stress–strain model for concrete confinement. *Engineering structures*, 48, 645–657.

- Chakrabarti, A., Chandra, A., & Bharagava, P. (2008). Finite element analysis of concrete columns confined with frp sheets. *Journal of reinforced plastics and composites*, 27(12), 1349–1373.
- Cheng, L., & Karbhari, V. M. (2006). New bridge systems using frp composites and concrete: a state-of-the-art review. *Progress in Structural Engineering and Materials*, 8(4), 143–154.
- Chung, K., & Lee, M.-G. (2018). *Basics of continuum plasticity*. Springer.
- Cristescu, N. D., Craciun, E.-M., & Soós, E. (2003). *Mechanics of elastic composites*. Chapman and Hall/CRC.
- Daniel, I. M., Ishai, O., Daniel, I. M., & Daniel, I. (2006). *Engineering mechanics of composite materials* (Vol. 1994). Oxford university press New York.
- Demir, A., Caglar, N., Ozturk, H., & Sumer, Y. (2016). Nonlinear finite element study on the improvement of shear capacity in reinforced concrete t-section beams by an alternative diagonal shear reinforcement. *Engineering Structures*, 120, 158–165.
- Erkmen, R. E., & Gottgens, B. (2018). A shell element for buckling analysis of thin-walled composite-laminated members. *International Journal of Structural Stability and Dynamics*, 18(02), 1850021.
- Farahmandpour, C., Dartois, S., Quiertant, M., Berthaud, Y., & Dumontet, H. (2017). A concrete damage–plasticity model for frp confined columns. *Materials and Structures*, 50(2), 1–17.
- Fattah, A. A. E. (2018). New axial stress-strain model of square concrete columns confined with lateral steel and frp. *Composite Structures*, 202, 731–751. doi: 10.1016/j.compstruct.2018.03.085
- fitnlm*. (n.d.). Retrieved from <https://www.mathworks.com/help/stats/fitnlm.html;jsessionid=d3a8b63ce136c1287ff60b24ca62>
- Ghernouti, Y., & Rabehi, B. (2011). Frp-confined short concrete columns under compressive loading: experimental and modeling investigation. *Journal of reinforced plastics and composites*, 30(3), 241–255.

- Grassl, P., & Jirásek, M. (2006). Damage-plastic model for concrete failure. *International journal of solids and structures*, 43(22-23), 7166–7196.
- Grassl, P., Lundgren, K., & Gylltoft, K. (2002). Concrete in compression: a plasticity theory with a novel hardening law. *International Journal of Solids and Structures*, 39(20), 5205–5223.
- Han, W., & Reddy, B. D. (2012). *Plasticity: mathematical theory and numerical analysis* (Vol. 9). Springer Science & Business Media.
- Hany, N. F., Hantouche, E. G., & Harajli, M. H. (2016). Finite element modeling of frp-confined concrete using modified concrete damaged plasticity. *Engineering Structures*, 125, 1–14.
- Ibrahimbegovic, A. (2009). *Nonlinear solid mechanics: theoretical formulations and finite element solution methods* (Vol. 160). Springer Science & Business Media.
- Ilki, A. (2006). Frp strengthening of rc columns (shear, confinement and lap splices). *BULLETIN-FIB*, 35, 123.
- Ilki, A., Peker, O., Karamuk, E., Demir, C., & Kumbasar, N. (2008). Frp retrofit of low and medium strength circular and rectangular reinforced concrete columns. *Journal of Materials in Civil Engineering*, 20(2), 169–188.
- Isleem, H. F., Wang, D., & Wang, Z. (2018). Modeling the axial compressive stress-strain behavior of cfrp-confined rectangular rc columns under monotonic and cyclic loading. *Composite Structures*, 185, 229–240.
- Jianguo, C., Jian, F., Jing, W., & Yunfeng, C. (2008). Behavior of frp-wrapped rectangular concrete columns. In *2008 international conference on information management, innovation management and industrial engineering* (Vol. 3, pp. 445–448).
- Karbhari, V. M., & Gao, Y. (1997). Composite jacketed concrete under uniaxial compression—verification of simple design equations. *Journal of materials in civil engineering*, 9(4), 185–193.
- Kelly, P. (2019). Mechanics lecture notes: An introduction to solid mechanics. Retrieved January, 25, 2019.

- Klisiński, M., & Mroz, Z. (1988). Description of inelastic deformation and degradation of concrete. *International journal of solids and structures*, 24(4), 391–416.
- Kollar, L. P., & Springer, G. S. (2003). *Mechanics of composite structures*. Cambridge university press.
- Krabbenhøft, K. (2002). Basic computational plasticity. *University of Denmark*.
- Lam, L., & Teng, J. (2003b). Design-oriented stress-strain model for frp-confined concrete in rectangular columns. *Journal of reinforced plastics and composites*, 22(13), 1149–1186.
- Lam, L., & Teng, J. G. (2003a). Design-oriented stress–strain model for frp-confined concrete. *Construction and building materials*, 17(6-7), 471–489.
- Lee, J., & Fenves, G. L. (1998). Plastic-damage model for cyclic loading of concrete structures. *Journal of engineering mechanics*, 124(8), 892–900.
- Lee, J.-Y., Oh, Y.-J., Park, J.-S., & Mansour, M. Y. (2004). Behaviors of concrete columns confined with both spiral and fiber composites. In *13th world conference on earthquake engineering* (Vol. 13).
- Lemaitre, J. (1985). A continuous damage mechanics model for ductile fracture.
- Lubliner, J., Oliver, J., Oller, S., & Onate, E. (1989). A plastic-damage model for concrete. *International Journal of solids and structures*, 25(3), 299–326.
- Matthys, S. (2000). *Structural behaviour and design of concrete members strengthened with externally bonded frp reinforcement* (Unpublished doctoral dissertation). Ghent University.
- Menetrey, P., & Willam, K. (1995). Triaxial failure criterion for concrete and its generalization. *Structural Journal*, 92(3), 311–318.
- Meschke, G., Lackner, R., & Mang, H. A. (1998). An anisotropic elastoplastic-damage model for plain concrete. *International journal for numerical methods in engineering*, 42(4), 703–727.
- Mirmiran, A., Zagers, K., & Yuan, W. (2000). Nonlinear finite element modeling of concrete confined by fiber composites. *Finite elements in analysis and design*, 35(1), 79–96.

- Moodi, Y., Mousavi, S. R., Ghavidel, A., Sohrabi, M. R., & Rashki, M. (2018). Using response surface methodology and providing a modified model using whale algorithm for estimating the compressive strength of columns confined with frp sheets. *Construction and Building Materials*, 183, 163–170.
- Ozbakkaloglu, T., Lim, J. C., & Vincent, T. (2013). Frp-confined concrete in circular sections: Review and assessment of stress–strain models. *Engineering Structures*, 49, 1068–1088.
- Ozbakkaloglu, T., & Saatcioglu, M. (2007). Seismic performance of square high-strength concrete columns in frp stay-in-place formwork. *Journal of Structural Engineering*, 133(1), 44–56.
- Papanikolaou, V. K., & Kappos, A. J. (2007). Confinement-sensitive plasticity constitutive model for concrete in triaxial compression. *International Journal of Solids and Structures*, 44(21), 7021–7048.
- Parvin, A., & Brighton, D. (2014). Frp composites strengthening of concrete columns under various loading conditions. *Polymers*, 6(4), 1040–1056.
- Pessiki, S., Harries, K. A., Kestner, J. T., Sause, R., & Ricles, J. M. (2001). Axial behavior of reinforced concrete columns confined with frp jackets. *Journal of composites for Construction*, 5(4), 237–245.
- Pham, T. M., & Hadi, M. N. (2014). Stress prediction model for frp confined rectangular concrete columns with rounded corners. *Journal of Composites for Construction*, 18(1), 04013019.
- Piscesa, B., Attard, M., Samani, A., & Tangaramvong, S. (2017). Plasticity constitutive model for stress-strain relationship of confined concrete. *ACI Structural Journal*, 114(2).
- Richart, F. E., Brandtæg, A., & Brown, R. L. (1929). *Failure of plain and spirally reinforced concrete in compression* (Tech. Rep.). University of Illinois at Urbana Champaign, College of Engineering
- Rousakis, T. C., & Karabinis, A. I. (2008). Substandard reinforced concrete members subjected to compression: Frp confining effects. *Materials and structures*, 41(9), 1595–1611.

- Rousakis, T. C., & Karabinis, A. I. (2012). Adequately frp confined reinforced concrete columns under axial compressive monotonic or cyclic loading. *Materials and structures*, 45(7), 957–975.
- Saafi, M., Toutanji, H., & Li, Z. (1999). Behavior of concrete columns confined with fiber reinforced polymer tubes. *Materials Journal*, 96(4), 500–509.
- Saatcioglu, M., & Razvi, S. R. (1992). Strength and ductility of confined concrete. *Journal of Structural engineering*, 118(6), 1590–1607.
- Samaan, M., Mirmiran, A., & Shahawy, M. (1998). Model of concrete confined by fiber composites. *Journal of structural engineering*, 124(9), 1025–1031.
- Sarikaya, A., & Erkmen, R. (2019). A plastic-damage model for concrete under compression. *International Journal of Mechanical Sciences*, 150, 584–593.
- Simo, J. C., & Hughes, T. J. (2006). *Computational inelasticity* (Vol. 7). Springer Science & Business Media.
- Simo, J. C., & Ju, J. (1987). Strain-and stress-based continuum damage models—i. formulation. *International journal of solids and structures*, 23(7), 821–840.
- Soden, P. D., Hinton, M. J., & Kaddour, A. (2004). Lamina properties, lay-up configurations and loading conditions for a range of fibre reinforced composite laminates. In *Failure criteria in fibre-reinforced-polymer composites* (pp. 30–51). Elsevier.
- Teng, J., Xiao, Q., Yu, T., & Lam, L. (2015). Three-dimensional finite element analysis of reinforced concrete columns with frp and/or steel confinement. *Engineering Structures*, 97, 15–28.
- Tsai, S. W. (1988). Composites design. *Think Composites, P. O. Box 581, Dayton, Ohio 45419, USA, 1988*. 583.
- Voyiadjis, G. Z., Taqieddin, Z. N., & Kattan, P. I. (2008). Anisotropic damage–plasticity model for concrete. *International journal of plasticity*, 24(10), 1946–1965.
- Yazdani, S., & Schreyer, H. (1990). Combined plasticity and damage mechanics model for plain concrete. *Journal of engineering mechanics*, 116(7), 1435–1450.

- Yu, T., Teng, J., Wong, Y., & Dong, S. (2010). Finite element modeling of confined concrete-ii: Plastic-damage model. *Engineering structures*, 32(3), 680–691.
- Zeng, J., Guo, Y., Li, L., & Chen, W. (2018). Behavior and three-dimensional finite element modeling of circular concrete columns partially wrapped with frp strips. *Polymers*, 10(3), 253.
- Zhang, D., Li, N., Li, Z.-X., & Xie, L. (2020). Experimental investigation and confinement model of composite confined concrete using steel jacket and prestressed steel hoop. *Construction and Building Materials*, 256, 119399.
- Zignago, D., Barbato, M., & Hu, D. (2018). Constitutive model of concrete simultaneously confined by frp and steel for finite-element analysis of frp-confined rc columns. *Journal of Composites for Construction*, 22(6), 04018064.